Studies of partonic distributions using semi-inclusive production of Kaons

K. Hafidi *†, J. Arrington, R. Dupré, D. F. Geesaman, R. J. Holt, D. H. Potterveld, P. E. Reimer, P. Solvignon

Argonne National Laboratory, Argonne IL 60439, USA

F. Benmokhtar †, Y. Van Haarlem

Carnegie Mellon University, Pittsburgh, PA 15213, USA

M. Battaglieri, R. De Vita, V. Drozdov, M. Osipenko, M. Ripani, M. Taiuti

INFN, Via Dodecaneso 33, 16146 Genova, Italy

M. Mirazita †, E. De Sanctis, L. Hovsepyan, S. A. Pereira, P. Rossi

INFN Laboratori Nazionali di Frascati, I-00044 Frascati, Italy

G. M. Urciuoli

INFN Roma I, I-00161 Rome, Italy

E. Cisbani, F. Cusanno, F. Garibaldi, S. Frullani

INFN Roma I and Istituto Superiore di Sanita, I-00161 Rome, Italy

R. De Leo, L. Lagamba, S. Marrone, E. Nappi, G. Simonetti, I. Vilardi

INFN Sezione di Bari and University of Bari, 70126 Bari, Italy

V. Bellini, G. Russo, M. L. Sperduto, C. M. Sutera

INFN - Sezione di Catania and Universita' di Catania, I-95123 Catania, Italy

A. D'Angelo, C. Schaerf, V. Vegna

INFN - Sezione di Roma Tor Vergata and Universita' di Roma Tor Vergata, I-00133 ROMA, Italy

H. Avakian †, V.D. Burkert, L.Elouadrhiri, V. Kubarovsky, S. Stepanyan

Jefferson Lab, Newport News, VA 23606, USA

CLAS12 Proposal *15 December 2008*

A. El Alaoui [†], E. Voutier

LPSC, Grenoble, CNRS/IN2P3, France

K. Joo, M. Ungaro

Physics University of Connecticut, Storrs CT 06269, USA

A CLAS collaboration proposal

[†] Co-spokesperson

[*] Contact: Kawtar Hafidi (kawtar@anl.gov)

Abstract

The proposed measurements are two-fold. First, we propose to measure the multiplicities for several hadron species ($\pi^+, \pi^-, \pi^0, K^+, K^-, K^0_s$) using both hydrogen and deuterium targets. The goal of these measurements is the control of the fragmentation functions used in the extraction of the individual quark and antiquark contributions to the nucleon spin. In addition to the measurement of the shape (x dependence) of the strange parton distribution function for several z and Q^2 bins with three independent measurements ($\pi^+ + \pi^-$, $K^+ + K^-$ and K^0_s). This part of the proposal can run simultaneously with the approved 12 GeV proposal to measure the magnetic form factor of the neutron in CLAS12. The second fold is the polarized measurements. The aim is to use two different methods to access the quark polarization. The first is the so called isoscalar method where only polarized deuterium is used to extract the non strange and strange polarized parton distribution functions. The second method is also a flavor decomposition method using the information on both hydrogen and deuterium targets to extract individual contributions of the quarks to the nucleon spin. This part of the proposal can run simultaneously with the already approved single and double spin asymmetry program in Hall B. Both polarized and unpolarized measurements will cover a x range from $0.05 < x < 0.7$. An important part of the proposed measurements requires a good charged kaon identification for the whole momentum range. Therefore, to enhance the existing good particle identification, one needs to seriously consider a RICH detector for CLAS12.

Contents

1 Collaborators commitment to the 12 GeV upgrade of Jefferson Lab

- Argonne National Laboratory Medium Energy group is actively involved in this proposal, as well as other proposals using CLAS12. Among CLAS12 baseline equipment, the group intends to take responsibility for the design, prototyping, construction and testing of the high threshold Cerenkov counter. Three research staff and two engineers are likely to work at least part time on this project in the next few years. Funding for the group is from DOE. Additional sources of funding will be sought as appropriate. Beyond the baseline equipment, the group is also interested in exploring the possibility of building a RICH detector for CLAS12.

- The Italian JLAB12 collaboration (INFN Bari, INFN Catania, Laboratori Nazionali di Frascati, INFN Genova, INFN Roma I and Istituto Superiore di Sanita', INFN Roma Tor Vergata) is actively involved in this proposal. Among CLAS12 equipment, the group plans to contribute to the design, prototyping, construction and testing of the CLAS12 RICH detector and central calorimeter. Seven staff members and three post-docs will spend their time as needed on this project. Funding for the group is from the Italian research agency Istituto Nazionale di Fisica Nucleare (INFN). Additional funding are planned to be sought in the European Community.

- The University of Connecticut (UConn) group is actively involved in this proposal using CLAS12 baseline equipment. Among the CLAS12 baseline equipment projects, the UConn group has taken responsibility for (1) the development of the CLAS12 detector simulation program based on Geant4-software-toolkit, and (2) the design, prototyping, construction and testing of the high threshold Cerenkov counter (HTCC). One faculty member (K. Joo), one research associate (M. Ungaro), six graduate students are already or will be working at least part time on the CLAS12 project for the next few years. The group is currently funded by the U.S Department of Energy (DOE) and the University of Connecticut Research Foundation (UCRF). Additional sources of funding will be sought as appropriate.

2 Introduction

Knowledge of Parton Distribution Functions (PDFs) represents the basis of our understanding of hadronic matter in terms of its fundamental degrees of freedom. A tremendous progress was made in the last two decades in the global analysis of PDFs where Deep Inelastic Scattering (DIS) experiments played a key role in providing high quality data covering a large kinematical map. However, much improvement is still needed in several areas. Perhaps the most surprising one is the strangeness sector. The lack of knowledge on the strange and anti-strange parton distributions, $s(x)$ and $\bar{s}(x)$, is reflected in the common practice in current global QCD analyses of PDFs of adopting the simplifying ansatz $s = \bar{s} = r(\bar{u} + \bar{d})/2$ [1] (where $\bar{u}$ and $\bar{d}$ are the up and down sea anti-quarks) at some low factorization scale. Even the proportionality constant r is only very loosely constrained by data. While the neutrino data [2–4] is considered to be useful, it does only offer limited information [5] on the normalization and the shape of the strange PDFs.

The knowledge of fragmentation functions which are the twin sisters of the PDFs is not in better shape although great progress was made recently with the *pp* measurements from RHIC and semi inclusive DIS measurements from HERMES. Where different hadron species were identified thanks to the RICH detector. The excellent particle identification of the HERMES experiment was key to the successful flavor tagging program allowing the direct determination of the contribution of individual quark, antiquark flavor to the nucleon spin.

In the proposed measurements, we will walk the same steps as HERMES did. We will use unpolarized hydrogen and deuterium data to measure the multiplicities for different hadron species, namely $(\pi^+, \pi^-, \pi^0, K^+, K^-, K^0_s)$. Here the kaons play an important role since they are very sensitive to the strange content of the nucleon. The multiplicity measurements are by themselves important. They carry a probabilistic information about hadronization process which is a non perturbative process. They are supposed to be universal. Therefore they can be used when needed regardless of the reaction in play. Knowing the multiplicities for different hadrons and in the same kinematical regime can reduce dramatically the systematic uncertainties inherent to the flavor decomposition methods used in the extraction of the individual quark polarization. Taking advantage of the x dependence of the measured multiplicities, one can get important information on the shape of the strange PDFs.

Having multiplicities under control, one can proceed to precise extraction of the individual quark helicity distributions via double spin asymmetry measurements . In this proposal, we would like to improve the statistical and the systematical precision of the existing measurements, especially for the sea quarks. Since the kaons are the most sensitive to the strange content of the nucleon, and their numbers are greatly reduced compared to pions, one needs to pay special attention to their identification.

To this end, a RICH detector for CLAS12 would be the perfect solution.

3 Physics Motivations

After many decades of extensive studies, understanding the nucleon internal structure remains on the top of the task list that physicists should address. Although a lot of progress has been made towards pinning down the quark-gluon structure of the nucleon, a full understanding of the origin of its spin has yet to emerge. The nucleon spin story started in the late 80's with a crisis when the European Muon Collaboration (EMC) at CERN found that contribution of the quark to the spin of the nucleon to be small and actually consistent with zero within the uncertainties [6]. Later, we realized that quarks are contributing 30% to the nucleon spin, leading to more important contribution for the quark orbital angular momentum and gluons. Although a part of the hadronic community switched gear toward measurements of the glue contribution to the nucleon spin, there is a general consensus that the job is far from done in the quark sector. The proof is the RHIC spin program (quark sector) and the spin studies at JLab 12 GeV upgrade.

Until recently, inclusive measurements have provided most of the current knowledge of nucleon spin structure. However, they are only sensitive to the sum of the quark and antiquark distribution functions because the scattering cross section depends on the squared charge of the quarks and antiquarks. The polarization of the individual flavors is only accessible in fits to inclusive data where additional assumptions are used such as SU(3) symmetry for the sea quarks. Accessing in more direct way the contributions from individual quarks and antiquarks can be achieved when hadrons are detected in the final state in addition to the scattered lepton. This method is called "flavor tagging" where the statistical correlation between the struck quark and the produced hadron "fragmentation function" is a key ingredient. HERMES experiment was pioneering in such measurements [7]. The extracted distributions $\Delta u(x)$ and $\Delta d(x)$ are consistent with inclusive results as shown in Fig. 1, but have better precision. The sea distributions were extracted separately for the first time and were found to be consistent with zero. The strange sea was found to be slightly positive but consistent with zero while the inclusive measurements yielded a negative value. An alternative method, the so-called isoscalar method was used to extract the strange sea distributions [8]. The result was found consistent with the five flavor decomposition with improved precision (see Fig. 2). The advantage of such method is its simplicity (isoscalar target), minimal assumptions and control of the systematic errors related to fragmentation functions because they can be determined from multiplicity measurements. As one can see, much has been done toward a complete understanding of the contributions of individual quarks to the nucleon spin. However, a lot of room is left for improvement, especially in the sea sector ($\Delta\bar{u}$, $\Delta\bar{d}$, Δs and $\Delta\bar{s}$). One can take advantage from the high luminosity available at JLab 12 GeV upgrade and improve the

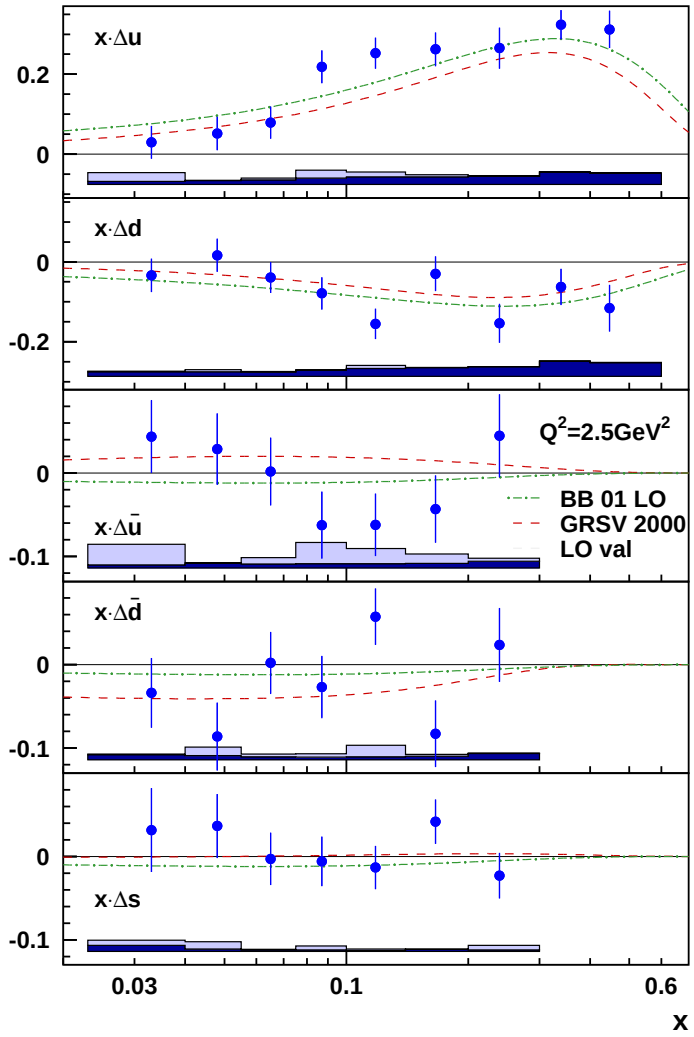

Fig. 1. The quark helicity distributions $x\Delta q(x)$ evaluated at $Q^2 = 2.5GeV^2$ as a function of x. The dashed line is the GRSV2000 parameterization [9] (LO,valence scenario) scaled with $1/(1 + \mathrm{R})$ and the dashed-dotted line is the Blümlein-Böttcher (BB) parameterization [10] (LO, scenario 1). Horizontal bands represent systematic uncertainties.

statistical precision especially in the kaon sector. Special attention should be given to K^- since it is a purely sea object that will allow us to avoid u-quark dominance. The authors in Ref. [11] suggested that measuring $A_{1p}^{K^-}$ is particularly sensitive to $\Delta\bar{u}-\Delta\bar{d}$. The quantity $\Delta\bar{u}-\Delta\bar{d}$ is of particular interest. It provides an excellent test for models which successfully describe the unpolarized densities $\bar{u} - \bar{d}$. Two of such models are the Chiral Quark Soliton Model (χQSM) [11], which is based on an effective theory where baryons appear as soliton solutions of the Chiral Lagrangian. The second one is a meson cloud model [12] that describes the nucleon as a bare nucleon and a cloud of virtual mesons. The two models have very distinct predictions for $\Delta\bar{u}-\Delta\bar{d}$. The only direct measurement of $\Delta\bar{u}-\Delta\bar{d}$ was performed by HERMES. The results are shown in Figure 3. While HERMES data tend to prefer flavor symmetry, no decisive conclusion can be made due to the lack of statistical precision. A recent global next-to-leading

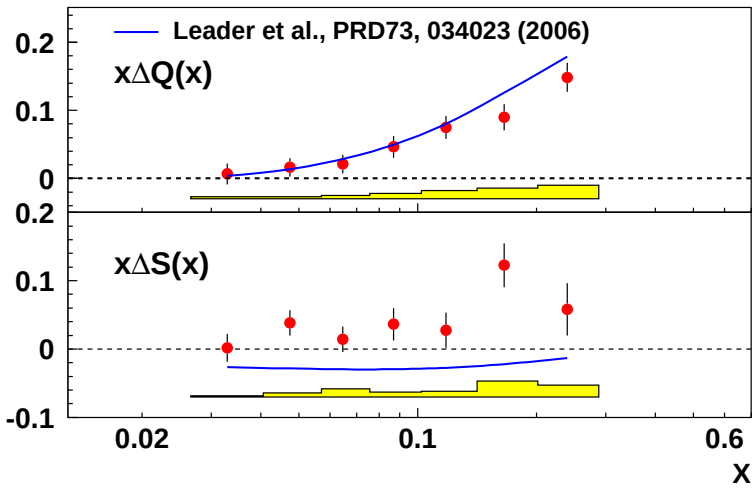

Fig. 2. Flavor decomposition results from HERMES experiment evolved to $Q^2 = 2.5$ GeV^2 using the isoscalar method. $x\Delta Q$ is the non strange polarized PDF while $x\Delta S$ is the strange one.

order analysis [13] of DIS, SIDIS, and preliminary RHIC data in terms of the helicity parton distributions, gives rise to a robust pattern for the sea polarizations, clearly deviating from SU(3) symmetry. Moreover, COMPASS leading order measurements of deuteron asymmetry [14] for charged hadrons $A^{h^+-h^-}$ combined with the first moment of g_1^d from the same measurements, favors a non-symmetric polarization of light quarks ($\Delta\bar{u} = -\Delta\bar{d}$) at a confidence level of two standard deviations. With the anticipated precision of the proposed measurements, one can clearly validate one if any of the existing models. Important ingredients in the flavor decomposition method are fragmentation functions (FFs). The knowledge of fragmentation functions has been rapidly evolving, following the path of parton densities, however without attaining yet their precisions. Up to recently, most of the information used to determine FFs comes essentially from electron-positron annihilation into charged hadrons. These data are precise and clean since they do not depend on parton densities. However, they do not give any information on how to disentangle the quark from antiquark fragmentation as they refer to the charge sum for certain hadron species such as $(\pi^+ + \pi^-)$. The information on how the individual quark fragments into hadrons depends crucially on the tagging techniques and the underlying assumptions implemented in the Monte Carlo generator used. Fortunately, in the last few years several measurements coming from both proton-proton collisions and deep-inelastic lepton-nucleon scattering have matured enough as to yield complementary information on the fragmentation process with competing precision [15–19]. These measurements were the main driver for excellent improvement of the FF parameterizations [20] where less stringent assumptions on the flavor asymmetry of FFs are made. The proposed measurements can contribute tremendously to this database with high quality multiplicity data for various hadron species $(\pi^+, \pi^-, \pi^0, K^+, K^-, K_s^0)$ off proton and deuteron. The high luminosity will allow us to perform two or three dimensional binning (x, z, Q^2) checking for example the Q^2 evolution of FFs. The same data can be used to reduce the

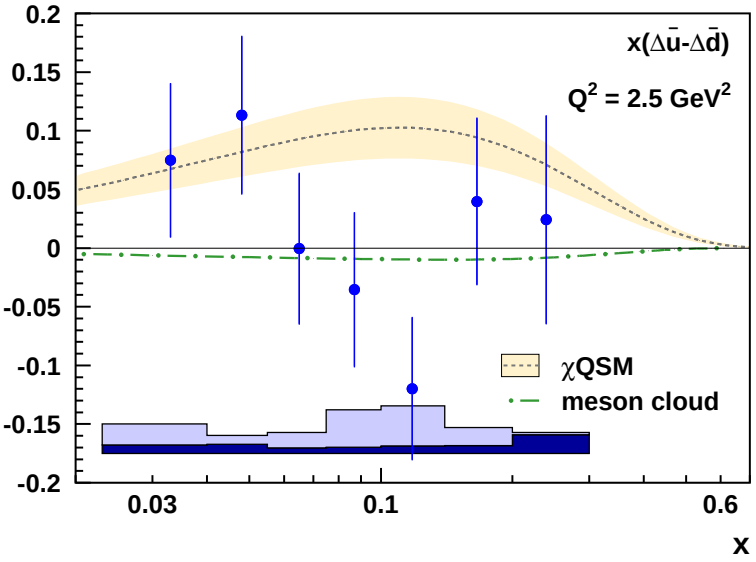

Fig. 3. $\Delta\bar{u} - \Delta\bar{d}$ from HERMES experiment evolved to $Q^2 = 2.5$ GeV^2. The data are compared with predictions in the χQSM [11] and a meson cloud model [12]. The solid line with the surrounding shaded band show the χQSM prediction with its $\pm 1\sigma$ uncertainties while the dash-dotted line shows the prediction in the meson cloud model. Horizontal bands represent systematic uncertainties.

systematic uncertainties in the extraction of the polarized parton distribution functions. It can also be used as was done recently by HERMES to determine the shape of the strange parton density distribution (see. Fig. 4) checking the assumption used in the parameterization about $s = \bar{s} \propto (\bar{u} + \bar{d})/2$.

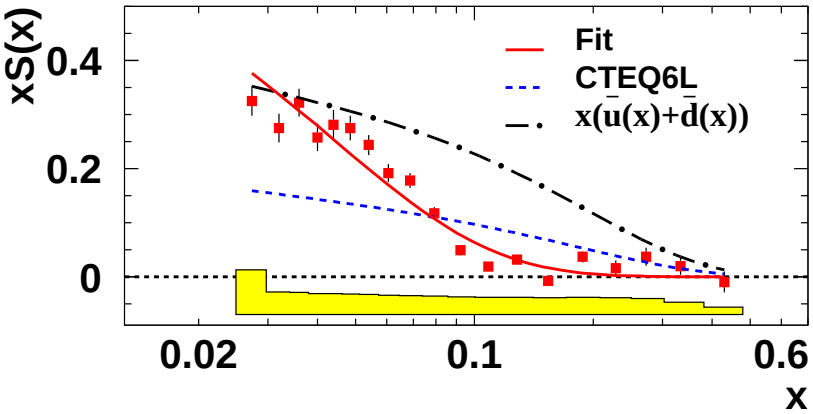

Fig. 4. HERMES strange PDF extraction from semi inclusive DIS data on deuteron. Horizontal bands represent systematic uncertainties.

4 Experimental Observables

This section is organized in the following manner. The first subsection describes the extraction method of the strange PDFs from measured multiplicities. This method is valid for unpolarized isoscalar targets such as deuterium and for specific final state such as ($K^+ + K^-$, $\pi^+ + \pi^-$ or K^0_s). The second subsection describes the formalism used to extract asymmetries and the strange helicity distributions using the so-called isoscalar method. Both the beam and the target are polarized longitudinally. The third subsection describes the flavor decomposition method using both polarized proton and deuteron targets to extract different flavor contributions to the nucleon spin.

4.1 Formalism for unpolarized deuteron target: Multiplicities and Strange PDFs

At the leading order of QCD and for unpolarized Semi Inclusive Deep Inelastic Scattering (SIDIS), the cross section for hadron production at a given x, Q^2 and z, normalized to the corresponding inclusive cross section takes the factorized form

$$\frac{d\sigma^h(x,Q^2,z)/dxdQ^2dz}{d\sigma^{DIS}(x,Q^2)/dxdQ^2} = \frac{dN^h(x,Q^2,z)}{dN^{DIS}(x,Q^2)} = \frac{\sum_q e_q^2 q(x,Q^2) D_q^h(z,Q^2)}{\sum_q e_q^2 q(x,Q^2)} \tag{1}$$

where q is the parton distribution function for a quark of a flavor q, e_q is its charge and D_q^h is the fragmentation function. D_q^h is a measure of the probability that a quark of a flavor q fragments into a hadron of type h. At moderate beam energies considered here, the sum is over quark and anti-quark flavors $q = (u, \bar{u}, d, \bar{d}, s, \bar{s})$. Here x is the dimensionless Bjorken scaling variable representing the momentum fraction of the target carried by the parton in the frame where the target has infinite momentum. Q^2 is the squared four-momentum of the exchanged virtual photon and $z = E_h/\nu$ is the fraction of the photon energy ν carried by the hadron of energy E_h. For deuterium; an isoscalar target, the fragmentation functions become isospin independent. By assuming isospin symmetry between proton and neutron, the strange PDF to be identical for both nucleons and charge conjugation invariance in the fragmentation functions, the multiplicity of Eq. (1) for a final product (H) takes the following form

$$\frac{dN^H(x,Q^2)}{dN^{DIS}(x,Q^2)} = \frac{Q(x,Q^2)\int D_{NS}^H(z,Q^2)dz + S(x,Q^2)\int D_S^H(z,Q^2)dz}{5Q(x,Q^2) + 2S(x,Q^2)} \tag{2}$$

where $H = K^+ + K^-$, $H = \pi^+ + \pi^-$ or $H = K^0_s$. The sum of non strange and strange parton distribution functions are $Q = u + \bar{u} + d + \bar{d}$ and $S = s + \bar{s}$ respectively. Furthermore, $D_{NS}^H = 4D_u^H + D_d^H$ and $D_S^H = 2D_s^H$ are the non strange and strange fragmentation functions respectively. In the denominator of Eq. (2), the term $2S(x,Q^2)$ is at the most 1% ($0.05 < x < 0.075$) of the $5Q(x,Q^2)$ term, therefore one

can safely drop it from the previous equation

$$\frac{dN^H(x,Q^2)}{dN^{DIS}(x,Q^2)} = \frac{Q(x,Q^2)\int D_{NS}^H(z,Q^2)dz + S(x,Q^2)\int D_S^H(z,Q^2)dz}{5Q(x,Q^2)} \tag{3}$$

If we contemplate carefully Eq. (3), we realize that once we are in the region where the sum of the strange parton distribution functions $S(x)$ vanishes, the multiplicity becomes independent of x

$$\frac{dN^H(x,Q^2)}{dN^{DIS}(x,Q^2)} = \frac{\int D_{NS}^H(z,Q^2)dz}{5} \tag{4}$$

Once in that region, one can extract for each z bin, the Q^2 dependence of the non strange fragmentation function from the measured multiplicities. By taking the non strange PDFs from recent parameterizations such as CTEQ6L and plugging the non strange fragmentation function into Eq. (3), one can extract the x dependence of strange contribution $S(x,Q^2)\int D_S^H(z,Q^2)dz$ for specific (z,Q^2) bins. This method is reliable in getting the information about the shape of the sum of the strange PDFs. However its absolute value $S(x,Q^2)$ relies on the quality of the used parameterization for the fragmentation functions.

4.2 Formalism for polarized deuteron target: Asymmetries and Strange helicity distributions

In a similar way as for the unpolarized case, the leading order double spin asymmetry (photon-nucleon) for SIDIS can be expressed as

$$A_1^h(x,Q^2,z) = \frac{\sum_q e_q^2 \Delta q(x,Q^2) D_q^h(z,Q^2)}{\sum_q e_q^2 q(x,Q^2) D_q^h(z,Q^2)} \tag{5}$$

where $\Delta q(x,Q^2)$ is the quark helicity distribution. Rewriting Eq. (5) in a more compact way using the so called purity formalism, one gets the factorized form

$$A_1^h(x,Q^2,z) = \sum_q \mathcal{P}_q^h(x,Q^2,z)\frac{\Delta q(x,Q^2)}{q(x,Q^2)} \tag{6}$$

where the expression for the purity is

$$\mathcal{P}_q^h(x,Q^2,z) = \frac{e_q^2 q(x,Q^2) D_q^h(z,Q^2)}{\sum_q e_q^2 q(x,Q^2) D_q^h(z,Q^2)} \tag{7}$$

The concept of purity can be generalized to inclusive scattering by setting the fragmentation function to unity in the expression of purity of Eq. (7). Moreover it can be applied to different targets (proton, deuteron) and hadron species (pions, kaons and

more). Now, when using isoscalar target such as deuterium, and limiting the produced hadrons to be either $H = K^+ + K^-$, $H = \pi^+ + \pi^-$ or $H = K^0_s$, in addition to the assumption of isospin symmetry between proton and neutron and charge conjugation invariance in the fragmentation functions ($D^H_u = D^H_{\bar{u}}$, $D^H_d = D^H_{\bar{d}}$, $D^H_s = D^H_{\bar{s}}$), the purity formalism simplifies to a linear relationship between the measured double spin asymmetries and the total non strange and strange quark helicity distributions. This relationship can be expressed as follow

$$\begin{pmatrix} A_d(x,Q^2) \\ \\ A^H_d(x,Q^2) \end{pmatrix} = C_R \begin{pmatrix} \mathcal{P}_{NS}(x,Q^2)\ \mathcal{P}_S(x,Q^2) \\ \\ \mathcal{P}^H_{NS}(x,Q^2)\ \mathcal{P}^H_S(x,Q^2) \end{pmatrix} \begin{pmatrix} \Delta Q(x,Q^2)/Q(x,Q^2) \\ \\ \Delta S(x,Q^2)/S(x,Q^2) \end{pmatrix}. \quad (8)$$

The inclusive purities given in terms of parton distributions have the simple form

$$\mathcal{P}_{NS}(x,Q^2) = \frac{5Q(x,Q^2)}{5Q(x,Q^2)+2S(x,Q^2)}, \quad \mathcal{P}_S(x,Q^2) = \frac{2S(x,Q^2)}{5Q(x,Q^2)+2S(x,Q^2)}. \quad (9)$$

The purities for the SIDIS aysmmetries include factors given by the appropriate fragmentation functions integrated over the measured range of z values,

$$\mathcal{P}^H_{NS}(x,Q^2) = \frac{Q(x,Q^2)\int D^H_{NS}(z,Q^2)dz}{Q(x,Q^2)\int D^H_{NS}(z,Q^2)dz + S(x,Q^2)\int D^H_S(z,Q^2)dz}, \quad (10)$$
$$\mathcal{P}^H_S(x,Q^2) = \frac{S(x,Q^2)\int D^H_S(z,Q^2)dz}{Q(x,Q^2)\int D^H_{NS}(z,Q^2)dz + S(x,Q^2)\int D^H_S(z,Q^2)dz}.$$

The strange and non-strange fragmentation functions of Eq. 10 are simple functions of the familiar fragmentation functions measured in collider experiments:

$$\int D_{NS}(z,Q^2)dz = 4\int D^H_u(z,Q^2)dz + \int D^H_d(z,Q^2)dz \quad (11)$$
$$\int D_S(z,Q^2)dz = 2\int D^H_s(z,Q^2)dz.$$

The factor $C_R \equiv (1+R)/(1+\gamma^2)$ in Eq. 8 compensates for the longitudinal photon contribution inherited from PDF parameterizations due to the fact that their fit is made to the F_2 structure functions while we obtain our PDFs from the A_1 asymmetries which are purely transverse. $R = \sigma_L/\sigma_T$ is the ratio of the longitudinal to the transverse virtual photon polarization and $\gamma = Q^2/\nu^2$. To solve Eq. 8, one needs to measure both the inclusive and semi inclusive asymmetries in addition to the inclusive and semi inclusive purities. The semi inclusive purities of Eq. 10 can be determined directly from the unpolarized multiplicities described earlier. While the inclusive ones shown in Eq. 9 need the input from the PDFs parameterizations. In the case of non strange PDFs, one can rely on the existing parameterizations. However, one should

be cautious for the strange PDFs. Luckily their contributions to the inclusive purities are quite small making them marginally sensitive to strange PDFs input.

4.3 Formalism for polarized proton and deuteron targets: flavor decomposition

One can write Eq. (5) in a matrix form

$$\overrightarrow{\mathcal{A}}(x,Q^2) = \mathcal{P}(x,Q^2) \cdot \overrightarrow{\mathcal{Q}}(x,Q^2) \tag{12}$$

The measured asymmetries in different bins in (x, Q^2) are elements of the vector $\overrightarrow{\mathcal{A}}$

$$\overrightarrow{\mathcal{A}}(x,Q^2) = (A_{1p}, A_{1p}^{\pi^+}, A_{1p}^{\pi^-}, A_{1p}^{K^+}, A_{1p}^{K^-}, A_{1p}^{K^0_s}, A_{1d}, A_{1d}^{\pi^+}, A_{1d}^{\pi^-}, A_{1d}^{K^+}, A_{1d}^{K^-}, A_{1d}^{K^0_s}) \tag{13}$$

The matrix $\mathcal{P}(x,Q^2)$ contains the purities for the proton and deuteron, while the vector $\overrightarrow{\mathcal{Q}}(x,Q^2)$ contains the quark and anti-quark polarizations:

$$\overrightarrow{\mathcal{Q}}(x,Q^2) = (\frac{\Delta u}{u}, \frac{\Delta d}{d}, \frac{\Delta s}{s}, \frac{\Delta \bar{u}}{\bar{u}}, \frac{\Delta \bar{d}}{\bar{d}}, \frac{\Delta \bar{s}}{\bar{s}}) \tag{14}$$

As shown in Eq. 7, the purities depend on the unpolarized PDFs and the fragmentation functions. For the fragmentation functions, one can constrain them using measured pion and kaon multiplicities in the same kinematical range from unpolarized proton and deuteron data in the same way as described in the first subsection. Eq. 12 becomes a set of equations evaluated in all (x, Q^2) bins. They can be solved to give the vector $\overrightarrow{\mathcal{Q}}(x,Q^2)$ by χ^2 minimization accounting for the correlations between the various asymmetries.

5 Experimental Setup

In the proposed measurements we are combining two running configurations. The first one is in concurrence with the already approved CLAS12 proposal E12-07-104 [21] to measure the neutron magnetic form factor using the quasi-elastic ratio on deuterium. The beam energy is 11 GeV and both hydrogen and deuterium targets are used simultaneously. Both beam and targets are unpolarized. This configuration is perfect for multiplicity and fragmentation function measurements. For asymmetry measurements, the running conditions will be the same as the already approved CLAS12 proposals for inclusive E12-06-109 [22] and semi inclusive E12-07-107 [23] DIS studies where both the beam and the targets are longitudinally polarized. The proposed measurements need very good kaon identification especially for momenta higher than 2.5 GeV which is missing when using only CLAS12 base equipment. A RICH detector will make particle identification at CLAS12 quite complete. In this section, we will briefly

summarize the experimental setup for both configurations in addition to a detailed description of ongoing simulations to optimize CLAS12 RICH detector parameters.

5.1 CLAS12

The standard CLAS12 spectrometer capabilities will have to be enhanced with a RICH detector. A whole subsection is dedicated to its description and performance. The central tracker will also be used for backward angle detection of protons and pions. In addition to its usual functions, the central tracker solenoid will also be used to provide magnetic field for the polarized targets. Additional informations on CLAS12 can be found in the document provided as an appendix to all CLAS12 proposals.

5.2 Targets

Both unpolarized and polarized hydrogen and deuterium targets will be used. Their detailed description and functioning can be found in the approved proposal E12-07-104 [21] for the unpolarized target and in the approved DIS program [22,23] for the polarized target.

5.2.1 Dual Target

We propose to use a collinear, dual-cell target containing deuterium (for the primary measurements of multiplicities and the extraction of the shape of strange PDF) and hydrogen (for fragmentation function measurements on proton). The dual-cell target will be similar in design to the one used for the CLAS measurements of G_M^n [24] during the E5 running period. A conceptual drawing of the target is shown in Figure 5. Each of the cells containing liquid will be 2 cm in length with a 1.0 cm gap in between. The length of the cells is designed to fit within the current design of the CLAS12 silicon vertex tracker. To measure effects due to different target positions, we will collect data with the targets in opposite cells from the default configuration.

5.2.2 Polarized Targets

The proposed experiment requires use of a polarized solid state target. The target will be polarized via the method of Dynamic Nuclear Polarization (DNP). This technique typically achieves a proton polarization of 80-90%, and a deuteron polarization of 30-40%. The nucleons in the target will be polarized either parallel or anti-parallel to the electron beam direction.

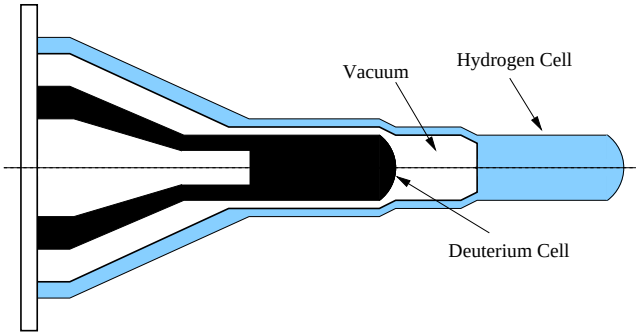

Fig. 5. The conceptual design of the dual-target cell (Courtesy of G. Gilfoyle).

The main systems required to realize DNP are the superconducting magnet to provide a strong (5 T) field, a ^{4}He evaporation refrigerator to maintain the target material at 1 K, a target insert which will house the target material and some additional instrumentation, a microwave system to transfer the polarization to the nucleon spins and a Nuclear Magnetic Resonance (NMR) system to determine the state of polarization.

In CLAS12 the polarizing magnetic field will be provided by the superconducting solenoid of the central detector. In this configuration, the central detector can be used also for polarized target experiments, yielding wide coverage for measurements of multi-hadron final states.

Ammonia and deuterated ammonia will be used as target material with the electron beam and CLAS12 (see Table. 1). (We will also investigate the possibility of using ^{6}LiD as a target material.) The ammonia will be frozen and broken up into small beads (to optimize the cooling surface) which fill the target cup. These targets offer high polarization, good resistance to radiation damage, and a relatively high ratio of polarizable nucleons per total number of nucleons. In order to determine the effective

Chemical Structure	$NH_3(ND_3)$
Target Diameter	up to 30 mm
Target Length	up to 100 mm
Density	0.917(1.056) g/cm^3
Dilution Factor	$\approx$ 0.15(0.22)
Packing Factor	$\approx$ 0.6

Table 1
Some Parameters of the Ammonia Targets

dilution factor f_{eff}, it will be necessary to collect data on the unpolarized material. A thin carbon target can be placed downstream in the same target cup for this purpose.

The target polarization will be monitored during the run via the NMR system, in the field of solenoid magnet. The calibration of the proton NMR can be done by mea-

surements of polarization in thermal equilibrium, taken with the polarizing magnet.

5.3 CLAS12 Particle Identification

In the baseline design of CLAS12, particle identification in the forward detector is obtained by using the high threshold Cerenkov counter (HTCC), the low threshold Cerenkov counter (LTCC) and the Time-of-flight scintillator arrays (TOF). In the $2.5-5$ GeV/c momentum region, the π/K separation relies only on the LTCC performance. Moreover, in the $4-8$ GeV/c momentum region it is not possible to separate protons from kaons. Considering that at 12 GeV for semi-inclusive processes, the K/π ratio is of the order of $10-15\%$ and assuming a pion detection inefficiency for the LTCC of 10%, then the π/K rejection factor is $1:1$. In general, this PID system is well matched to requirements of the main physics program at 12 GeV. However there are some physics reactions of high interest, such as the one covered by this proposal, that cannot be easily accessed without better PID, especially for charged kaon detection. A RICH detector, to be installed in place of the low threshold Cerenkov counter, will significantly improve the CLAS12 particle identification overcoming the above limitations.

5.3.1 CLAS12 RICH detector

A proximity focusing RICH similar to the one operating in Hall A at Jefferson Lab [25,26] and successfully working during the hyper-nuclear spectroscopy experiment [27], may represent an adequate choice to fulfill our requirements. Presently, we didn't take into account other possibilities, such as an aerogel RICH, due to the higher costs and additional technical constraints. A proximity focusing RICH detector will allow us a good separation of $\pi/K/p$ in the $2.5-5$ GeV/c momentum region, as demonstrated later on and, in addition, replacing part or full LTCC will not have any impact on the baseline design of CLAS12. Moreover, replacing LTCC with RICH has an advantage that it can be done module by module without interfering with detector construction of CLAS12 operations. In Fig. 6 a schematic layout of the proximity focusing RICH is reported. In the RICH operating in Hall A the photons are produced by over threshold particles in the liquid freon C_6F_{14} with a refractive index of 1.28 and thickness of 15 mm. Then they refract on a quartz window of 5 mm and diverge in a 160 mm proximity gap, filled by CH_4. Eventually they are converted to electrons by a thin layer of CsI (300 nm) deposited on five pad planes that represent the cathode of a Multi-wire Proportional Chamber. The induced charge of the electric avalanche is readout on each pad by a sample and hold analogically multiplexed front-end electronics. Spatial information is obtained from the segmented pads, whose size is $8\times8.4\ mm^2$. One of the most important aspect of the proximity focusing fluorocarbon/CsI RICH detector is represented by the deposition of a layer of photo-converted

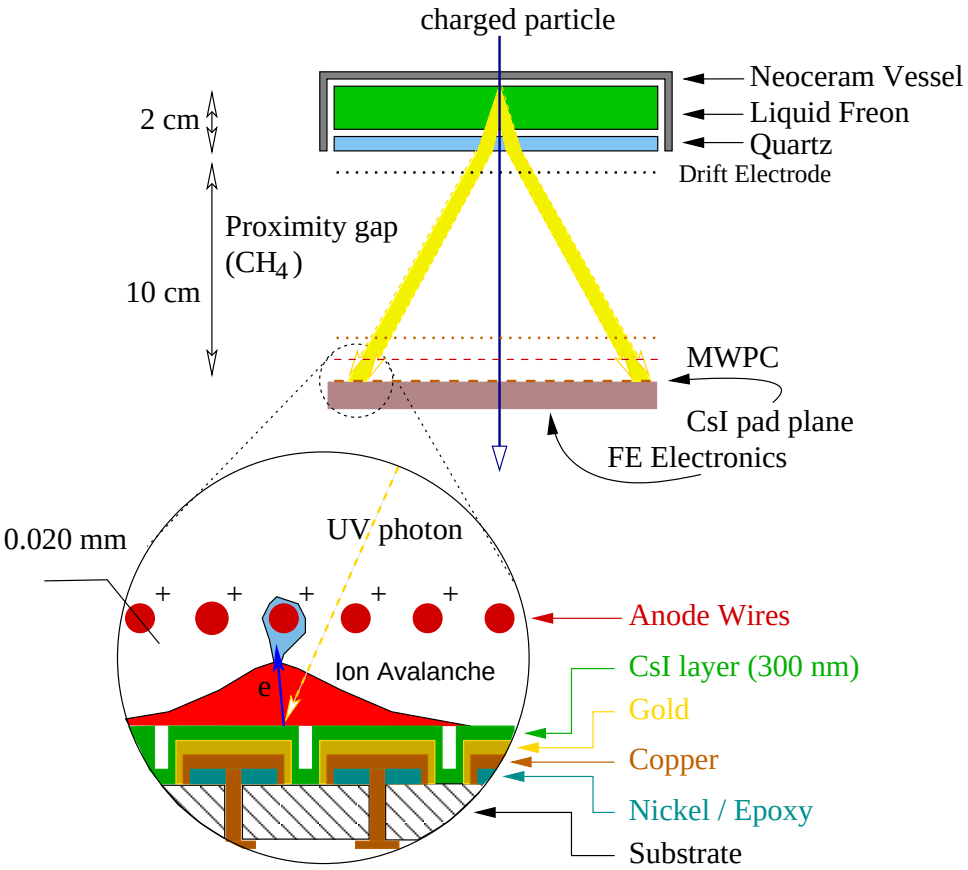

Fig. 6. Schematic layout and working principle of the freon CsI proximity focusing RICH.

material (CsI) on the pad plane. This is obtained by means of the evaporation of a pure CsI powder or crystals in a high vacuum chamber. The INFN Rome group has built, installed and operated at JLab an evaporation chamber for large area pad (up to about 650 x 650 mm^2). A quantum efficiency (QE) online measurement system has also been integrated into the evaporation chamber. A typical measured QE is of the order of $20 - 25$ %.

Preliminary Monte Carlo studies based on GEANT3 [28] has been performed in order to optimize all the components of the detector: radiator thickness, gap length, radiator type. The main output parameter will be the mean error on Cerenkov angle reconstruction of kaons and pions; $\sigma_{K-\pi}$.

Assuming particles uniformly distributed in the phase space, results obtained for kaon-proton and kaon-pion separation versus the particle momentum are shown in Fig 7 for two different radiators, C_5F_{12} and C_6F_{14}, respectively. In the plots the points refer to the Monte Carlo simulation while the curves are analytical functions. As we can see for the C_6F_{14} the $\sigma_{K-\pi}$ and σ_{K-p} are $\sim$ 1 mrad larger than for the C_5F_{12} thus the use of the latter is mandatory. The disadvantage in using the freon C_5F_{12} is its need for cooling because it evaporates at 29° Celsius at standard temperature

and pressure. In the simulation, the dimensions of the radiator thickness and the gap

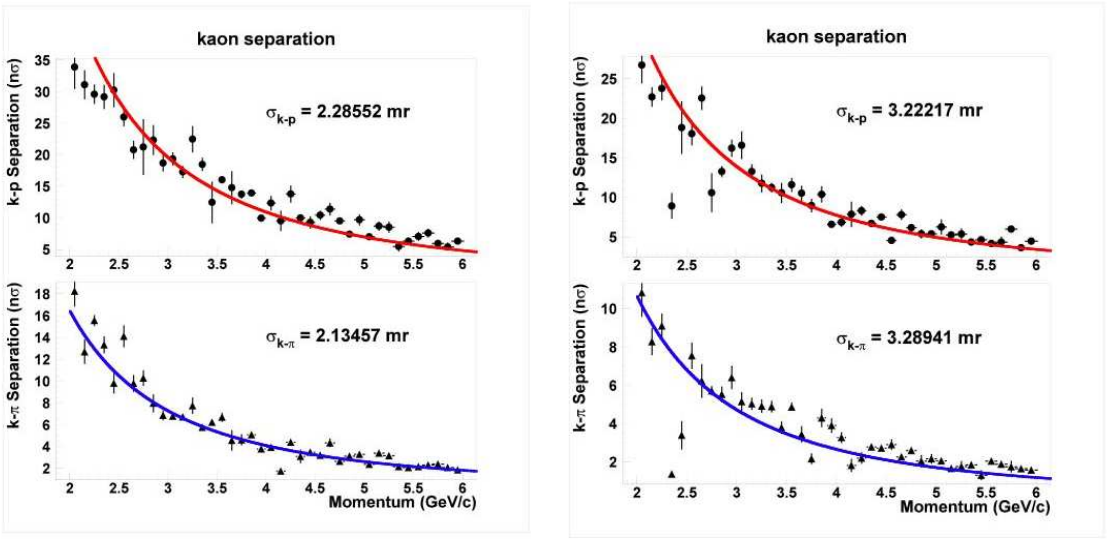

Fig. 7. Left: Kaon-proton separation (upper plot) and kaon-pion separation (lower plot) versus the particle momentum for C_5F_{12}. The points refer to the Monte Carlo simulation while the curves are analytical functions. Right: Kaon-proton separation (upper plot) and kaon-pion separation (lower plot) versus the particle momentum for C_6F_{14}. The points refer to the Monte Carlo simulation while the curves are analytical functions.

length as well as the pad/pixel size of the photon detector have been varied in order to find the optimal combination which gives the smaller reconstruction error in the Cerenkov angle. It has been found that a freon thickness of ~ 3 cm, a gap length of ~ 80 cm and a pad size less than 1 cm minimize the $\sigma_{K-\pi}$ value. Finally, to determine

Table 2
Radiation lengths corresponding to the different parts of the RICH detector.

	Thickness (cm)	$X_0\%$
Entrance window		
Al	0.05	0.5
Rohacell51	5	2
Al	0.05	0.5
Radiator		
Neoceram	0.4	3
C_6F_{14}	3	15
Quartz	0.5	4
Gap		
CH_4	80	0.001
Photon Detector		
Pad NEMAG10	0.08	0.4
or		
GEM chamber	1	0.6

the best photon detector size, pions, kaons and protons have been generated at the LTCC-RICH entrance window according to realistic phase space distributions. The positions at the detector level of all photons generated in the radiator has been studied

for a radiator polar angle acceptance of $5^\circ - 30^\circ$. In Fig. 8 left, the black dots are the charged particle positions at the RICH entrance (the envelope is the radiator). The contour lines are the positions at the detector level of all photons generated in the radiator (different colors refer to different intensity) while the large arc is the detector surface (photons outside of there are not detected). Our final results for the mean error on the kaon Cerenkov angle reconstruction are shown in Fig. 8 (Right). We can achieve a 4σ $K-\pi$ separation at 5 GeV/c. Therefore, we will have 80% kaon detection efficiency with 1:1000 rejection factor (or 95% with 1:100 rejection factor). This study was performed for a single sector of CLAS12, with a radiator size $\leq 4m^2$ and a detector size of $\sim 14m^2$. For six sectors, the radiator size will be $\leq 24m^2$ while the detector size of $\sim 40m^2$. The total radiation thickness of the proposed RICH is

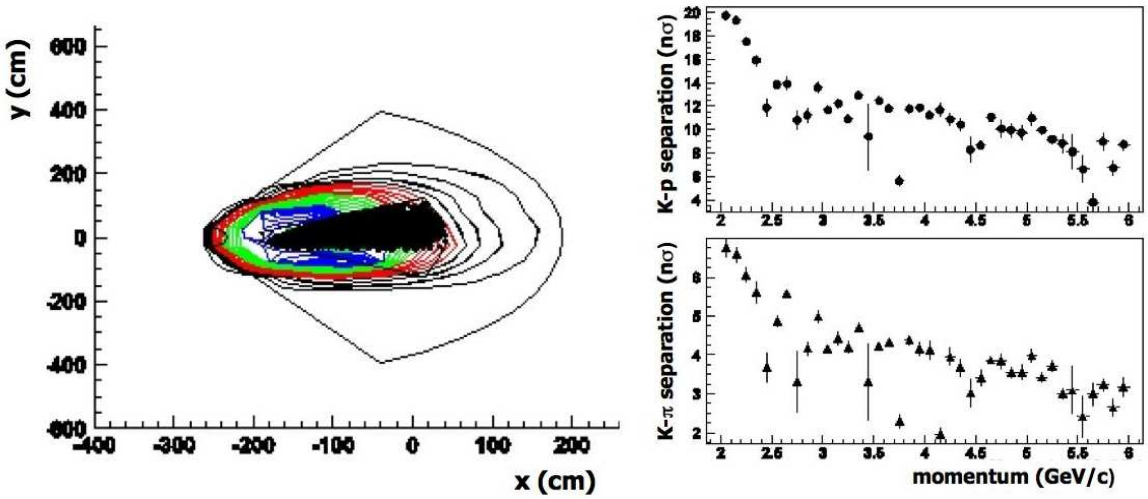

Fig. 8. Left: Contour lines: positions at the detector level of all photons generated in the radiator for a polar angle acceptance of $5^\circ - 30^\circ$. The black dots are the charged particle positions at RICH entrance; the large arc is the detector surface. x/y are not to scale. Right: Kaon-proton separation (upper plot) and kaon-pion separation (lower plot) versus the particle momentum for C_5F_{12} and a radiator polar angle acceptance of $5^\circ - 30^\circ$.

of the order of 30% X_0. In Table 2, the radiation lengths corresponding to different parts of the RICH detector are reported. A very preliminary cost estimate has been evaluated, based on the cost of the Hall A RICH detector. Taking into consideration the replacement of two adjacent LTCC sectors, it is found to be of the order of 2.5 M$. The crucial part to be funded is the liquid radiator C_5F_{12} for which a 0.8 M$ cost has been estimate (for the total quantity needed we have considered 5 times the volume of two sectors which is ~ 250 l). Detailed information about the proposed RICH, its cost and parameters can be found in Ref. [29].

5.3.2 Kaon Identification with CLAS12 with TOF, LTCC and HTCC

A simulation was performed to study kinematic dependences of kaons detected using the Time-of-flight scintillator arrays (TOF) at low momenta ($P < 2.5$ GeV) and the

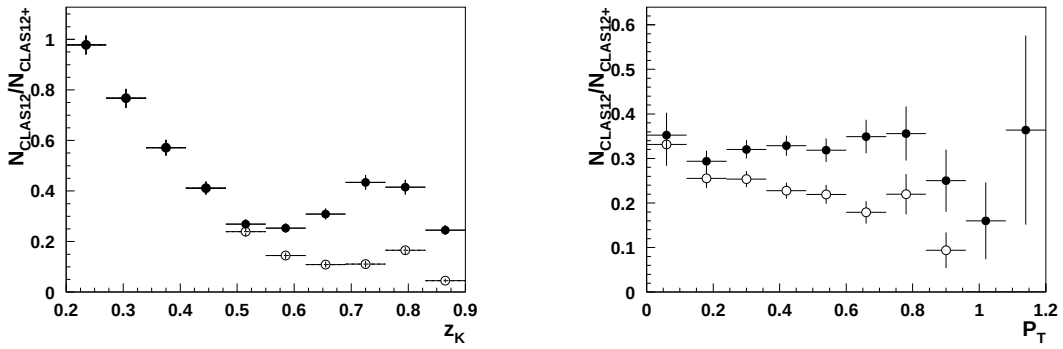

Fig. 9. Relative gain of kaons with CLAS12 (with RICH) compared to the base CLAS12. The open circles assume only Kaons detected by TOF ($P < 2.5$ GeV), filled circles include both TOF and HTCC ($P > 5$ GeV). The left plot shows the z dependence while the right one shows the P_T distribution.

high threshold Cerenkov counter at high kaon momenta ($P > 5$ GeV), assuming very high efficiency of the HTCC for pion detection. The relevant kinematic variables for semi-inclusive DIS are the x, y, z and the hadron transverse momentum with respect to the virtual photon P_T. While detection (identification) of kaons even in limited momentum range ($P < 2.5$ GeV and $P > 5$ GeV) will still allow a full coverage over the most accessible kinematics (see Fig.9) the statistics will be significantly less and distributions will be distorted. This is better seen for the the z and P_T-dependences of kaons, which are the most sensitive variables to the kaon momentum. The sectors of CLAS12 with no RICH will still provide a valuable for kaon studies data, but data from sectors covered by RICH will be very important to use them efficiently.

5.3.3 Advantages of the RICH

The best solution to improve K^+ and K^- identification and increase the statistics ($\sim$ a factor of 3) will be complimenting the PID system of forward detector with a Ring Imaging Cerenkov counter.

The time of flight can separate between kaons and protons for momenta up to 4 GeV/c. The kaon to proton ratio obtained from PEPSI Monte-Carlo is shown in Fig. 10 in the region where time of flight is not helpful. The number of proton is at least twice the number of kaons making the argument for a RICH detector even stronger.

In addition to much needed PID for kaons at momenta $P > 2.5$ GeV, RICH will help to reduce accidental in high luminosity runs, when particles from different beam buckets can mix. In Fig. 11 leakage of protons (left graph) and pions (right graph) from different beam buckets into kaons is illustrated. At high luminosities, protons

and pions that get produced at high rates will leak into kaon sample and measuring on TOF will not be enough to separate them.

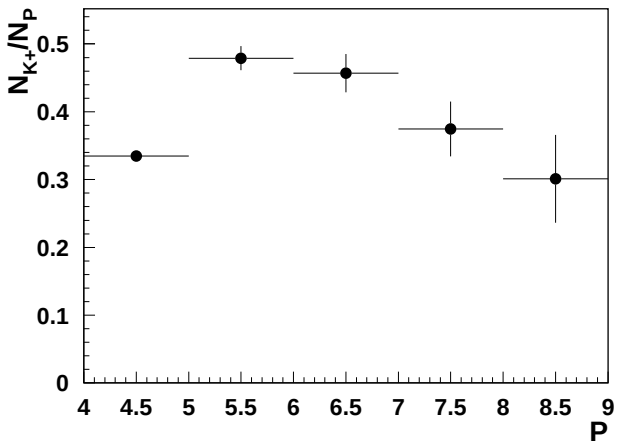

Fig. 10. The ratio of K^+ to proton as a function of the momentum from CLAS12-DIS Monte-Carlo.

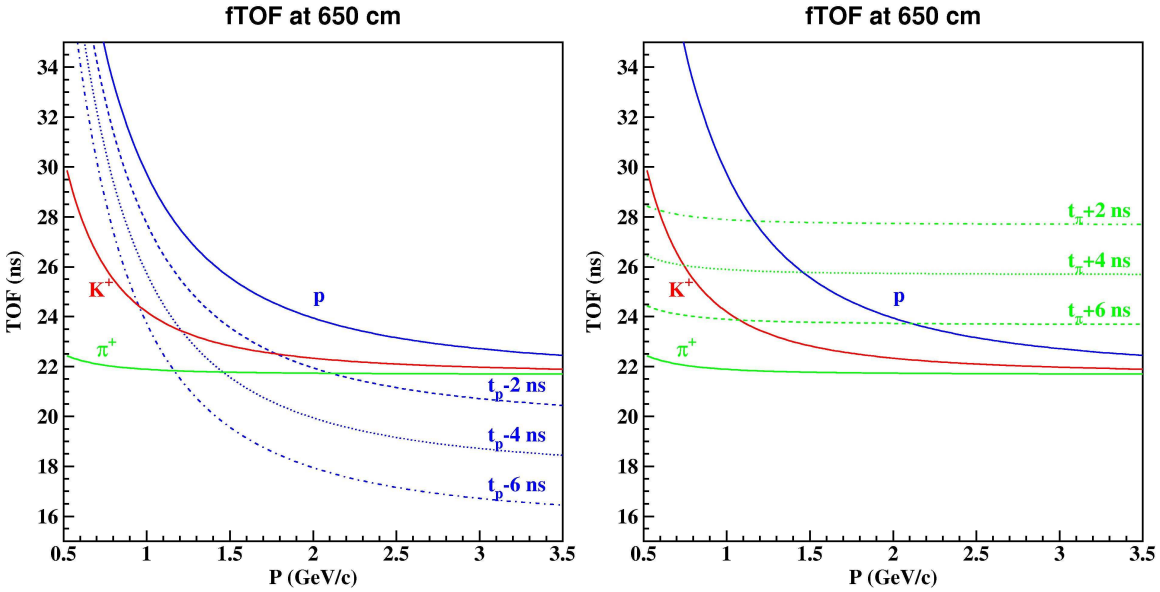

Fig. 11. Time-of-flight of π^+s (green lines), K^+s (red lines), and protons (blue lines) from the target to the FTOF plane as a function momenta. On the left (right) graph - dashed line, dotted line, and dashed-dotted line correspond to protons (pions) from previous (next) beam buckets leaking into kaon samples

6 Measurements

For both experimental configurations (unpolarized and polarized running), we are interested in the study of Semi Inclusive Deep Inelastic Scattering (SIDIS) off proton and deuteron, where the produced hadron is detected in coincidence with the scattered electron. The hadrons of interest are π^+, π^-, π^0, K^+, K^- and K^0_s. One can remove misidentified pions using the fits to the distribution of photo-electrons in the high threshold Cerenkov counter and the ratio of the energy deposited in the calorimeter to the measured momentum. One can also clean up the electron sample by removing electrons coming from pair-symmetric decays (e.g $\pi^0 \rightarrow e^+e^-$ or $\pi^0 \rightarrow \gamma e^+e^-$ as well as $\gamma \rightarrow e^+e^-$ conversions). While pion identification is very good at CLAS, we cannot say the same for kaons; especially K/p separation for momenta above 4 GeV. Following the preliminary studies for a CLAS12 RICH detector, detection efficiency is considered to be 80% for kaons with momenta above 3 GeV and two sectors coverage with a polar angle from 5 to 30 degrees. This coverage in polar angle is quite appropriate since all the kaons scattering at angles larger than 30 degrees have momenta below 3 GeV (see Fig. 12) where time of flight technique can be used successfully.

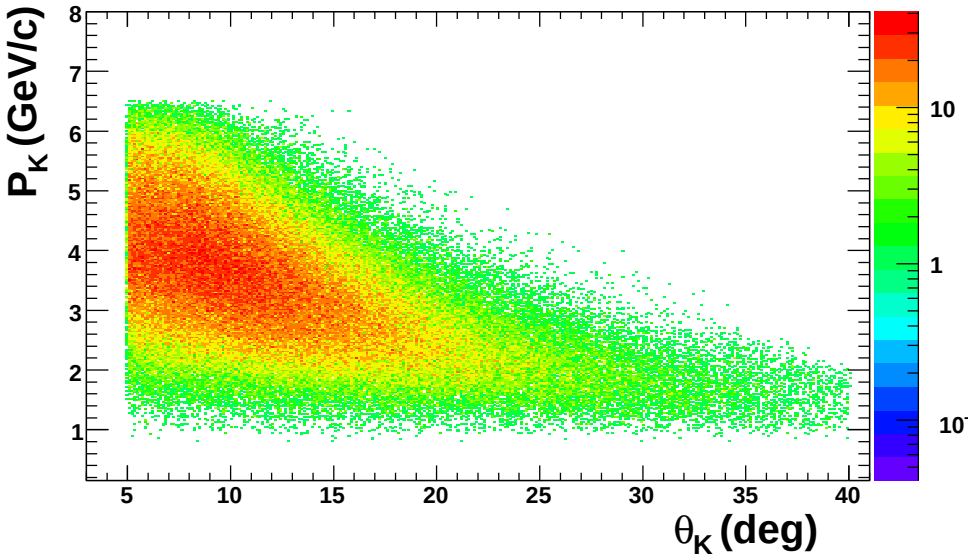

Fig. 12. Momentum versus polar angle for kaons generated using PEPSI Monte Carlo and accepted in CLAS12 for hadrons with $0.4 \leqslant z \leqslant 0.7$.

Figure 13 shows a two dimensional plot for x versus Q^2 in addition to the z distribution for kaons. For this measurements, we restrict the analysis to the z region between 0.4 and 0.7. The reason for the lower z cut is to avoid as much as possible the target fragmentation region. While the upper z limit is to reduce the contamination from pions coming from the ρ decay.

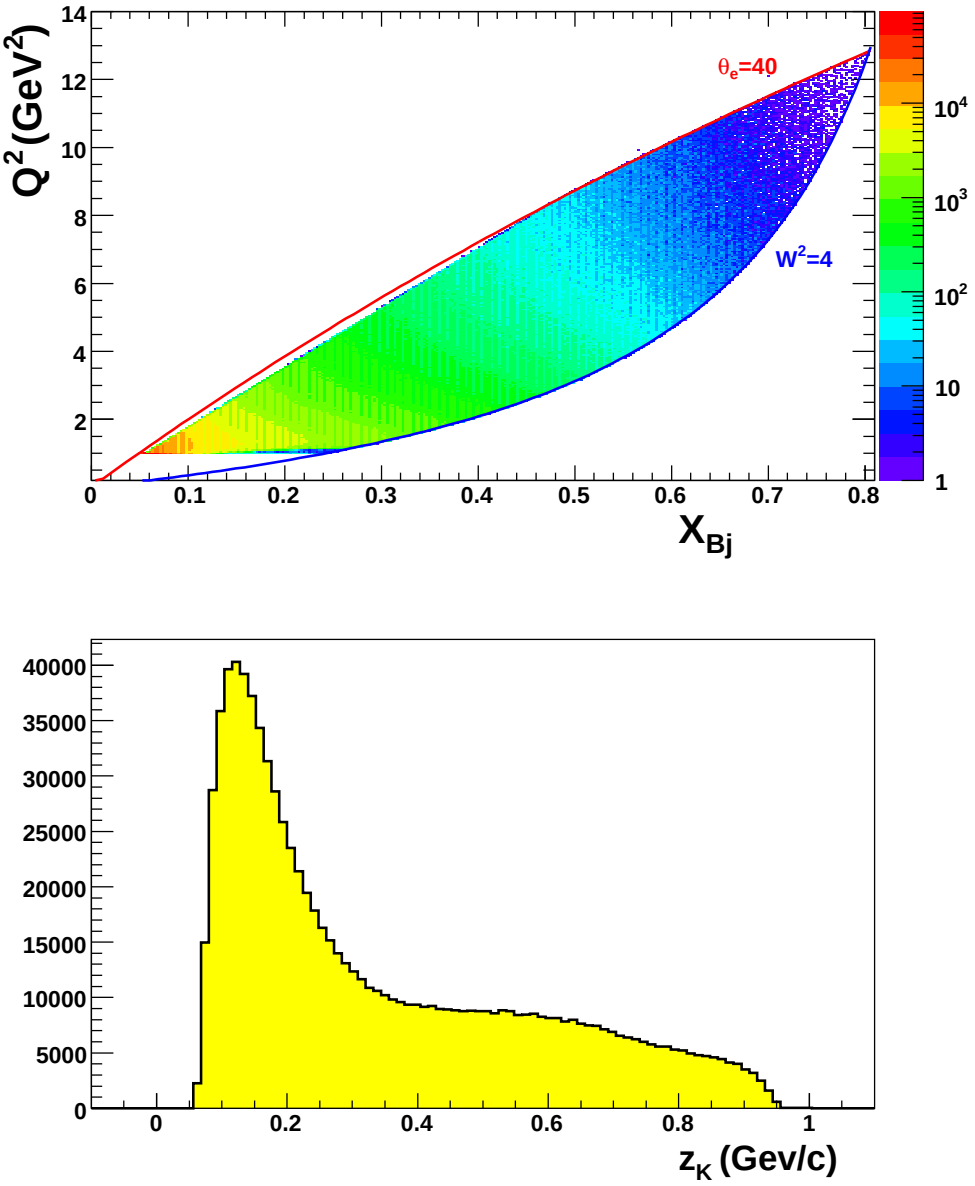

Fig. 13. Upper panel: x versus Q^2 distribution for kaons generated using PEPSI Monte Carlo and accepted in CLAS12. Lower panel: z distribution for kaons generated using PEPSI Monte Carlo and accepted in CLAS12.

Different kinematical distribution for K_s^0 are shown in Fig. 14. Due to its short lifetime ($\tau = 8.9$ ns), K_s^0 will be identified via its two pions decay with a branching ratio of 69%. To enhance the K_s^0 signal to background ratio, one can take advantage from the event topology illustrated in Fig 15. First one can determine the position of the decay vertex (secondary vertex) using the distance of the closest approach from the two pions tracks. The primary vertex can be determined from the reconstructed K_s^0 track given by the sum of the two pions three momenta vector. The flight distance

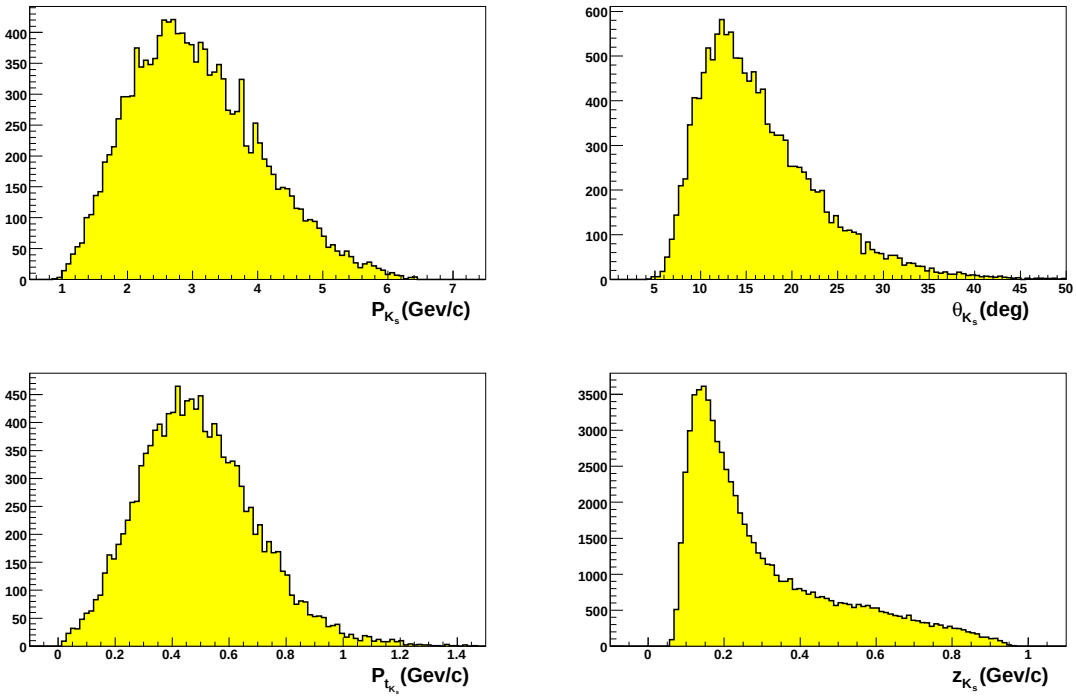

Fig. 14. K_s^0 kinematical distributions generated using PEPSI Monte Carlo and accepted in CLAS12.

"d" (the distance between the two vertices) for a K_s^0 of 1 GeV momentum is around 10 cm. Using this information, one can make a cut on $c\tau = M_{K_s^0} d / P_{K_s^0}$. In addition one can also constrain the angle between the direction of K_s^0 momentum and the vector defined with the two vertices to be very small.

6.1 Multiplicity Measurements

Although one can in principle combine different helicity states from the polarized data to extract hadron multiplicities, it is not preferable in our case since we will have to make nuclear corrections due to the nature of the polarized targets. The situation will be totally favorable if one can use successfully frozen spin HD targets. For now, we are considering the possibility of running simultaneously with the G_M^n experiment in Hall B. This means taking data with both hydrogen and deuterium targets in the beam. While this configuration is excellent for ratio measurements with the caution to switch the two targets for the control of acceptance corrections, it has no harm for the kind of measurements we would like to carry out, namely multiplicity measurements off hydrogen and deuterium targets.

One can see throughout the proposal that we are concentrating on deuterium measurements for the unpolarized part. Yet, we have also the intention to take full advantage

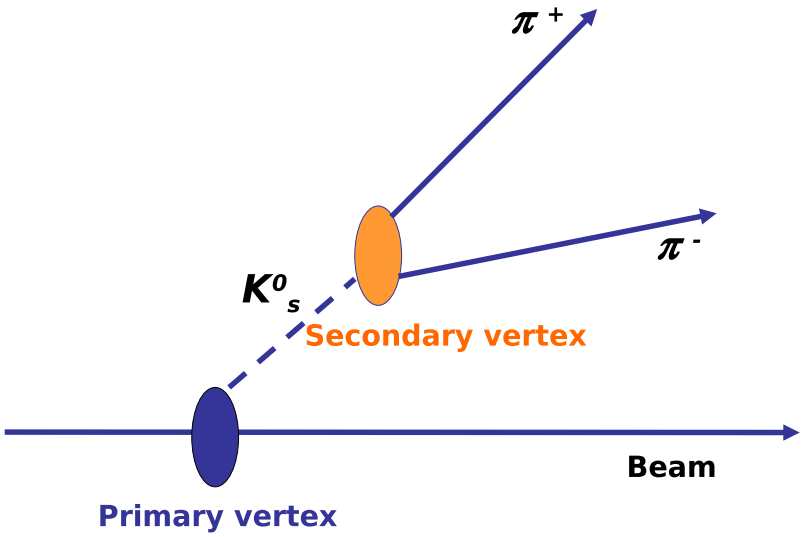

Fig. 15. The topology of a K_s^0 event.

of the hydrogen data that we will get automatically if we run in the dual-target configuration. Collecting high statistics hydrogen and deuterium data (especially with good particle identification capabilities) covering a large range in x, Q^2 and z is extremely valuable for constraining the Monte Carlo and tuning its parameters when used to compute the purities for flavor separation of the polarized PDFs. These data will also make important contribution to the existing multiplicity database used in the extraction of fragmentation functions hoping that one day we can get as precise FFs parameterization as their PDFs twins.

Already with the existing CLAS resolution, one can separate without any trouble the two target vertices which are 2 cm long and 2 cm apart. Moreover one can cut the contributions from the aluminum windows of the target cells. The amount of the material in the aluminum windows is about 3% of the material in the deuterium target. We will be keeping only events where the scattered electron was detected by itself or in coincidence with one or more of the following hadrons (π^+, π^-, K^+ or K^-).

The data will consist of counts N^{DIS} and (N^{π^+}, N^{π^-}, N^{K^+}, N^{K^-}, $N^{K_s^0}$) for different (x, Q^2) and (x, Q^2, z) bins respectively. From these counts, one can form the raw multiplicity ratios that will have to be corrected from radiative effects, particle identification inefficiencies, detector resolutions, in addition to 4π acceptance correction, to finally obtain the final born multiplicity distributions $dN^{K^+ + K^-}/dN^{DIS}$, $dN^{\pi^+ + \pi^-}/dN^{DIS}$ and $dN^{K_s^0}/dN^{DIS}$. Therefore for each (z, Q^2) bin, one can study the x dependence of the multiplicity. Mapping out the x-dependence will allow us to find the region where the multiplicity becomes independent of x and test whether this

value is independent of Q^2. Once we reach that region, which means that the strange PDFs vanished, we can integrate over all the corresponding x bins and extract the non-strange fragmentation functions $D_{NS}^{K^+ + K^-}$, $D_{NS}^{\pi^+ + \pi^-}$, and $D_{NS}^{K_s^0}$ as function of Q^2 for different z bins following Eq (4).

Now, using the non strange PDFs from CTEQ6L, one can extract the x dependence of the "strange terms" $S(x,Q^2) \int D_S^{K^+ + K^-}(z,Q^2)dz$, $S(x,Q^2) \int D_S^{\pi^+ + \pi^-}(z,Q^2)dz$ and $S(x,Q^2) \int D_S^{K_s^0}(z,Q^2)dz$ in Eq (3) for a specific (z,Q^2) bin. These terms carry important information about the shape of the strange PDFs, which can be directly compared to the CTEQ6L parameterization. One can further use DSS parameterization for the strange fragmentation functions $D_S^{K^+ + K^-}(z,Q^2)$, $D_S^{\pi^+ + \pi^-}(z,Q^2)$ and $D_S^{K_s^0}(z,Q^2)$ and deduce the quantity $x\Delta S(x)$ from three independent measurements.

6.2 Asymmetry Measurements

The double asymmetry measurements can be performed in parallel with previously accepted E12-06-109 and E12-07-107 proposals. A polarized beam (85% polarization as it is routinely achieved in recent JLab experiments) of about 10 nA on a 3 cm long ammonia target will be used. The resulting luminosity is of 10^{35} cm^{-2} s^{-1}. The beam will be rastered over the diameter of the target to minimize the dose density. The beam helicity will be flipped in a pseudo-random pattern every 33 ms. The standard Hall B beam devices will be used to monitor and stabilize the beam intensity and position, thus reducing any helicity correlated beam asymmetries to less than 10^{-3}.

A coincidence between the high threshold Cerenkov counter and a signal above threshold (corresponding to at least 1 GeV energy deposited) in the electromagnetic calorimeter in the same sector defines the first-level trigger. The high electron threshold will play an important role for reducing contaminations mainly from pions. If needed a level 2 trigger can be implemented requiring an electron candidate track in the same sector drift chamber as for level trigger. The total event rate in the DIS region for these measurements is expected to be around 2 kHz for Q^2 above 1 GeV^2. CLAS12 maximum data acquisition rate is about 20 kHz. A data acquisition rate of 10 kHz has already been achieved in CLAS DAQ.

The data will consist of a number of counts for the two beam helicity states (N^+ and N^-) parallel and anti-parallel to the longitudinal target polarization. Those counts will be normalized to the dead time and the integrated beam charge. One can then calculate the asymmetry ratio $A_{||}^{Raw} = (N^+ - N^-)/(N^+ + N^-)$. To get the final asymmetry, one has to divide the $A_{||}^{Raw}$ by the product of the beam and target polarization and the dilution factor. The dilution factor can be calculated from a detailed model of the target content and a parameterization of the world data on unpolarized structure function for nucleons and nuclei (^{15}N, ^{4}He, and C and Al foils) in the target,

including radiative effects. The only ingredient needed is the packing fraction (the fraction of the cell volume occupied by the ammonia beads), which can be extracted by comparing the rate from ammonia to that from an auxiliary carbon target. Additional measurements on empty and liquid-helium only targets will also be needed. Past experience with the EG1 experiment in Hall B have shown that a typical error of 3% on the dilution factor can be achieved [30]. An additional correction for the small polarization in ^{15}N and contamination by ^{14}N and, in the case of the deuterated ammonia, H, will be applied as well.

The beam (P_B) and target (P_T) polarization will be independently measured using Möller scattering and NMR, respectively. However, we can extract the product $P_B * P_T$ with higher precision directly from our data, by measuring the asymmetry of elastic (quasi-elastic) scattering $\vec{p}(\vec{e}, e'p)$ ($\vec{d}(\vec{e}, e'p)$) from our NH_3 (ND_3) targets, respectively. We did a full simulation of this method, including radiative effects, CLAS12 acceptance and expected beam parameters. We find that the uncertainty on $P_B * P_T$ for the proton will be about 1% and on the deuteron about 3%.

7 Expected Results

The expected number of counts and corresponding statistical errors in the following subsections are based on a full simulation of inclusive and semi-inclusive deep inelastic scattering with the CLAS12 acceptance folded in. Events were generated with the CLAS12-DIS generator [31]. This generator is basically an implementation of the LUND Monte Carlo package called PEPSI (Polarized Electron-Proton Scattering Interactions) [32]. It is based on polarized and unpolarized parton distribution functions and the LUND string model for hadronization, and has been tested successfully against several low-Q^2 experiments with 5.x GeV beam at Jefferson Lab.

A fast Monte Carlo simulation program has been used to define the acceptance and resolution of the CLAS12 detector with all of the base equipment in place. The events generated by CLAS12-DIS are used as input and all particles are followed through all detector elements. The results of our simulation have been cross-checked with direct cross section calculations and a simple geometric acceptance model. The resolution of the detector is simulated by a simple smearing function which modifies a particle's track by a random amount in momentum and angles according to a gaussian distribution of the appropriate width. The amount of smearing follows the design specifications of the CLAS12 detector. In any case, a full Monte Carlo simulation (GEANT-based) of CLAS12 with all resolution effects will have to be used to determine the effective mean x and Q^2 for each x-bin we will use to bin our data so we can accurately extract the x-dependence of the measured asymmetries.

The usual DIS cuts were applied to the simulated data, namely $Q^2 \geqslant 1$ GeV^2, $W \geqslant$

2 GeV and $y = \nu/E \leqslant 0.85$. The y cut is usually used to reduce the region where radiative corrections are large.

7.1 Multiplicities

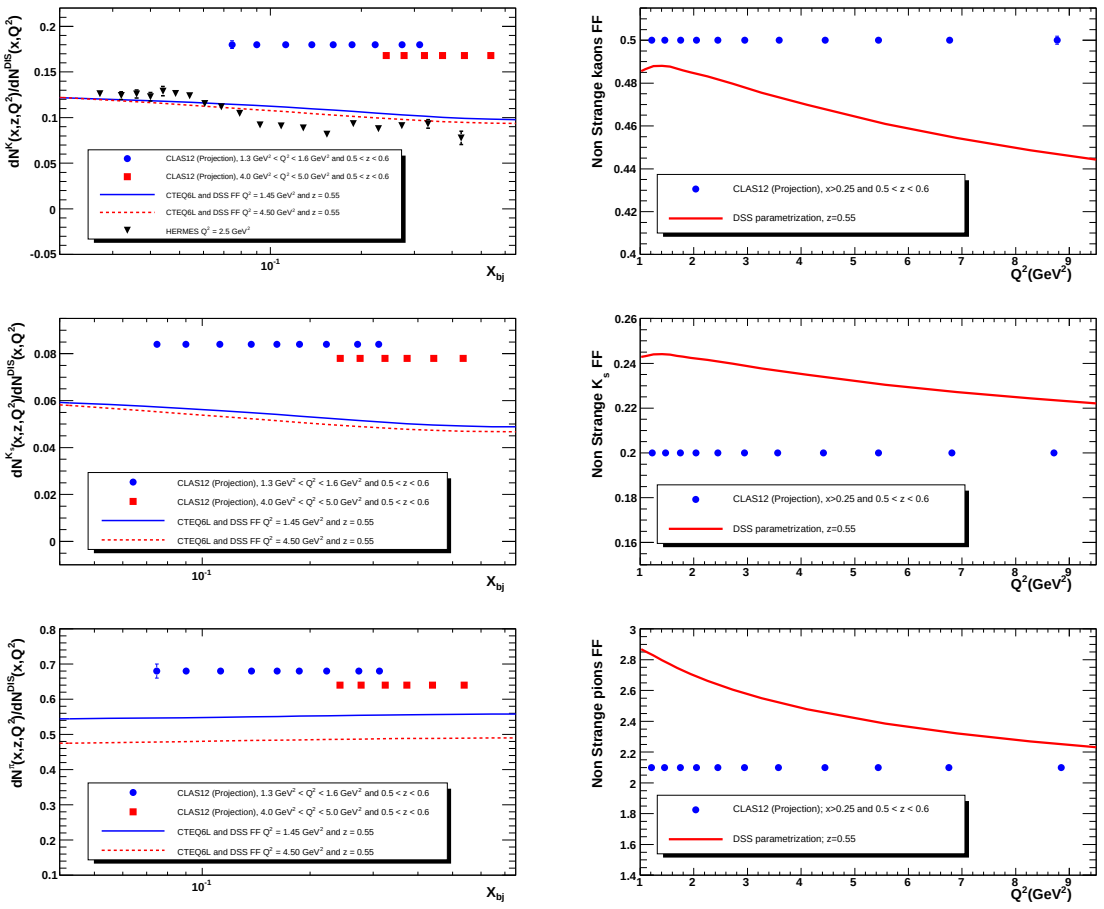

Fig. 16. Upper panel: Left (Right): Statistical projections for the x dependence of $K^+ + K^-$ multiplicity at fixed z bin and for two Q^2 bins (Statistical projections for Q^2 dependence of $K^+ + K^-$ non strange fragmentation function at fixed z bin). Middle panel: Left (Right): The same as the upper panel but for K^0_s. Lower panel: Left (Right): The same as the upper panel but for $\pi^+ + \pi^-$.

To obtain the final multiplicities, one has to apply several corrections. They include charge symmetric background correction, smearing, acceptance and radiative corrections. One should also correct for contributions from diffractive vector mesons such as ρ-meson for pions and ϕ-meson for kaons. For systematic uncertainties, most of them will drop since the measurements are ratios from the same target but one should keep in mind those related to RICH inefficiencies. To estimate them, one can use vector meson decay data where the ID of the decay product is known then check the RICH response. At this stage, it is too early to put a number. However, one should keep

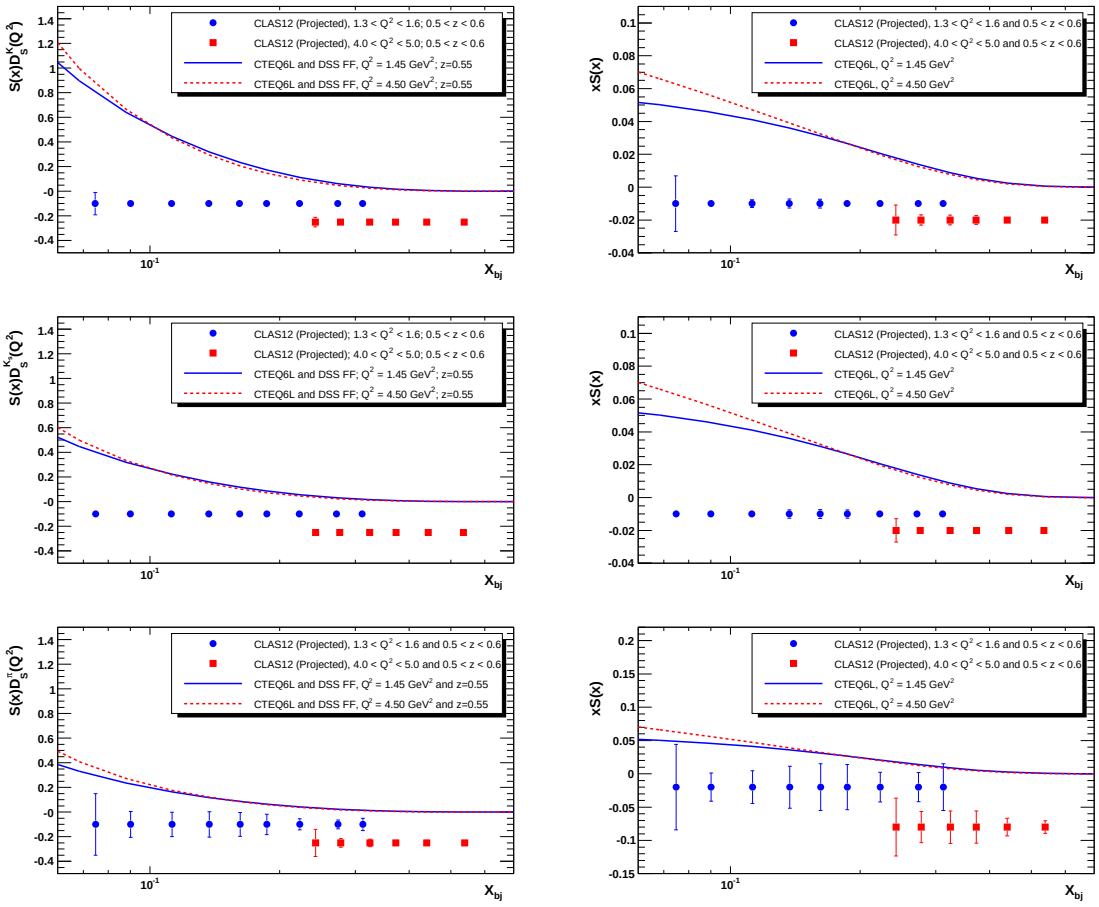

Fig. 17. Upper panel: Left (Right): Statistical projections for the x dependence of $K^+ + K^-$ ($S \times D_S$) at fixed z bin and for two Q^2 bins (Statistical projections for (xS) at fixed z bin and for two Q^2 bins from kaons data). Middle panel: Left (Right): The same as the upper panel but for K^0_s. Lower panel: Left (Right): The same as the upper panel but for $\pi^+ + \pi^-$.

it in mind when designing the RICH detector. The statistical errors are calculated assuming the already accepted 54 days of running with the G^n_M experiment with 0.5×10^{35} cm^{-2} s^{-1} and 80% RICH kaon detection efficiencies. Only a RICH coverage of two sectors was considered. Figure 16 shows statistical projections for the sum of kaons, K^0_s and the sum of pions respectively, along with multiplicity predictions using CTEQ6L for PDFs and DSS parameterization [33] for the fragmentation functions. We are only showing two bins in Q^2 but we have a total of 11 bins spanning the Q^2 range from 1 to 10 GeV^2. Assuming that the strange sea will vanish for $x > 0.25$, we have extracted the non strange fragmentation function D_{NS} as a function of Q^2 for the single $0.5 < z < 0.6$ bin. The same can be done for the other z bins. The projected statistical errors for the three final state are also shown in Fig. 16. The strange term ($S \times D_S$) projections for the same final states are shown in Fig. 17. The projected statistical errors on the strange term for pions are large because of the large value of the pion multiplicities that is also reflected on the absolute error. This result is expected because of the small strangeness content in the pions. The precision

on the kaons measurements will allow us to study the Q^2 dependence of the shape of the strange term. Given a normalization value which is the strange fragmentation function, one can get the strange PDF mainly from kaons since pions have small sensitivity as illustrated in Fig 17.

7.2 Asymmetries

Table 3
Uncertainties for asymmetry measurements.

Item	A_1^d
beam x target polarization	2%
depolarization and R	4%
dilution factor	3%
radiative corrections	3%
transverse (to γ^*) spin effects	3%

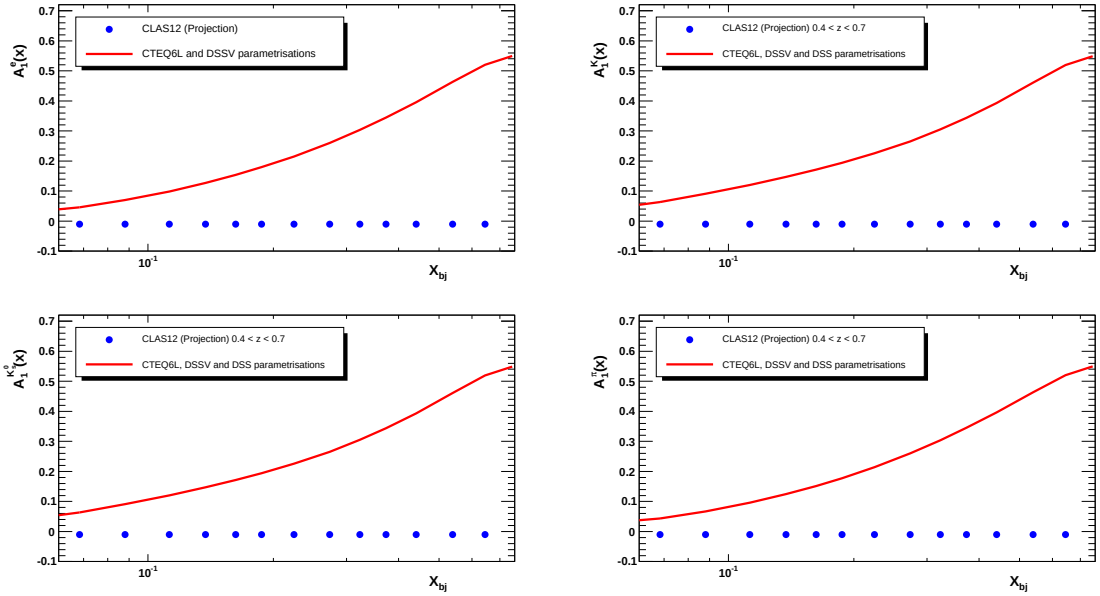

Fig. 18. Upper panel: Left (Right): Statistical projections for deuterium inclusive asymmetry (Statistical projections for deuterium kaon asymmetry). Lower panel: Left (Right): The same as the upper panel but for K_s^0 (pions).

The proposed spin asymmetry measurements are rather insensitive to uncertainties in

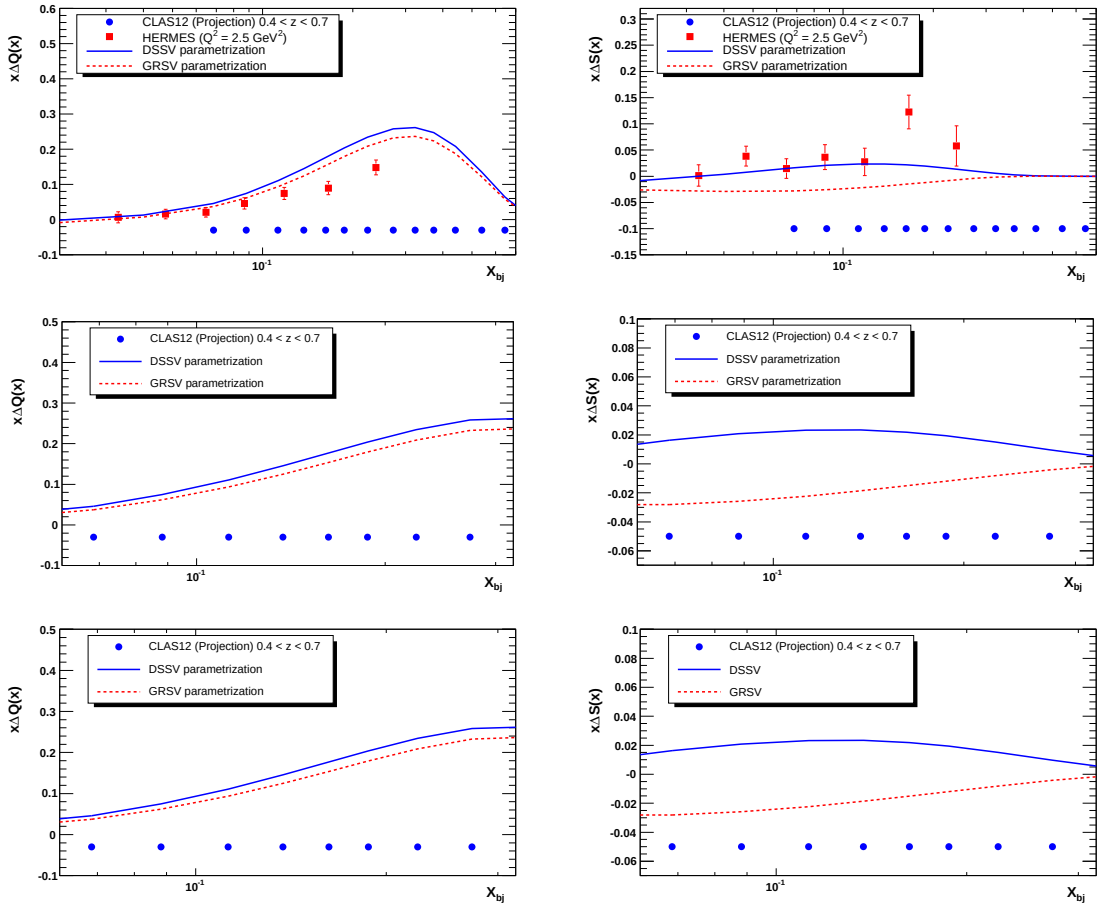

Fig. 19. Upper panel: Left (Right): Statistical projections for $x\Delta Q$ from kaon data including errors from multiplicities. Statistical projections for $x\Delta S$ from kaon data including errors from multiplicities. Middle panel: Left (Right): The same as the upper panel but for K^0_s. Lower panel: Left (Right): The same as the upper panel but for $\pi^+ + \pi^-$.

acceptances and charge normalization. The main systematic error is due to possible contamination of the single pion sample with pions from decays of exclusive vector mesons. For kaons, RICH misidentification will also come to play. Other sources of systematic errors include the beam and target polarizations, dilution factor and the longitudinal to transverse photo-absorption cross section ratio, $R(x, Q^2)$. The main sources of systematic errors in measurements of double spin asymmetries are listed in the Table 3. These errors are all scale errors, so are proportional to the size of the measured asymmetry. Studies of other sources of systematics, related to physics background, including target fragmentation, semi-exclusive processes, exclusive vector meson contributions and higher twist require the data of this measurement. We base our predicted statistical errors in the following sections on the assumption of running 30 days on NH_3 and 50 days on ND_3, where half of the time we will be running with two opposite torus fields. The reason behind is that we will gain a factor of two in the number of K^- while the number of K^+ will stay the same. This is due to the fact that in the electron-outbending configuration, the Q^2 distribution shifts

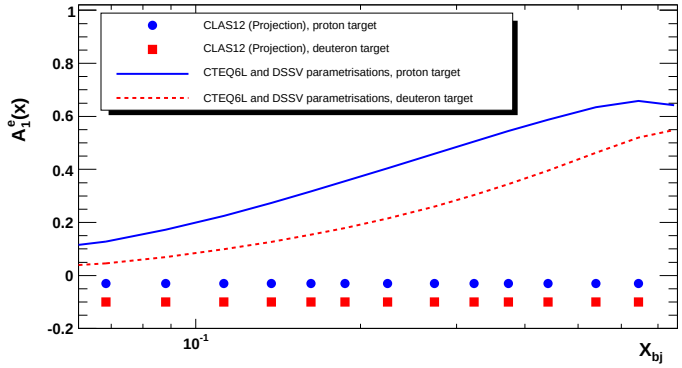

Fig. 20. Statistical projections for inclusive asymmetries on proton and deuteron.

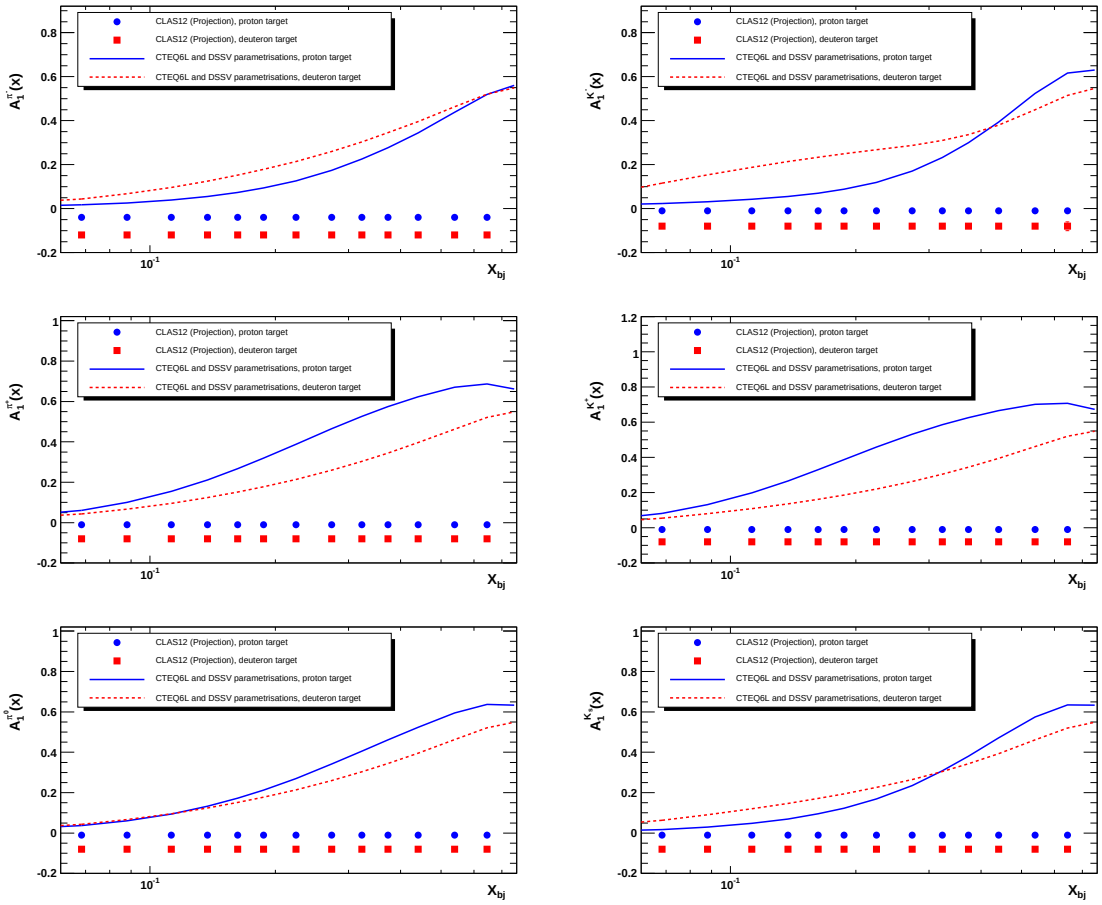

Fig. 21. Upper panel: Left (Right): Statistical projections for π^- asymmetry (K^-). Middle panel: Left (Right): Statistical projections for π^+ asymmetry (K^+). Lower panel: Left (Right): Statistical projections for π^0 asymmetry (K^0_s).

to lower values ($Q^2 > 1GeV^2$) where the cross sections are larger. The number of days was chosen identical to the already approved proposals E12-06-109 and E12-07-107. For our estimate of the total systematic error, we have added the systematic

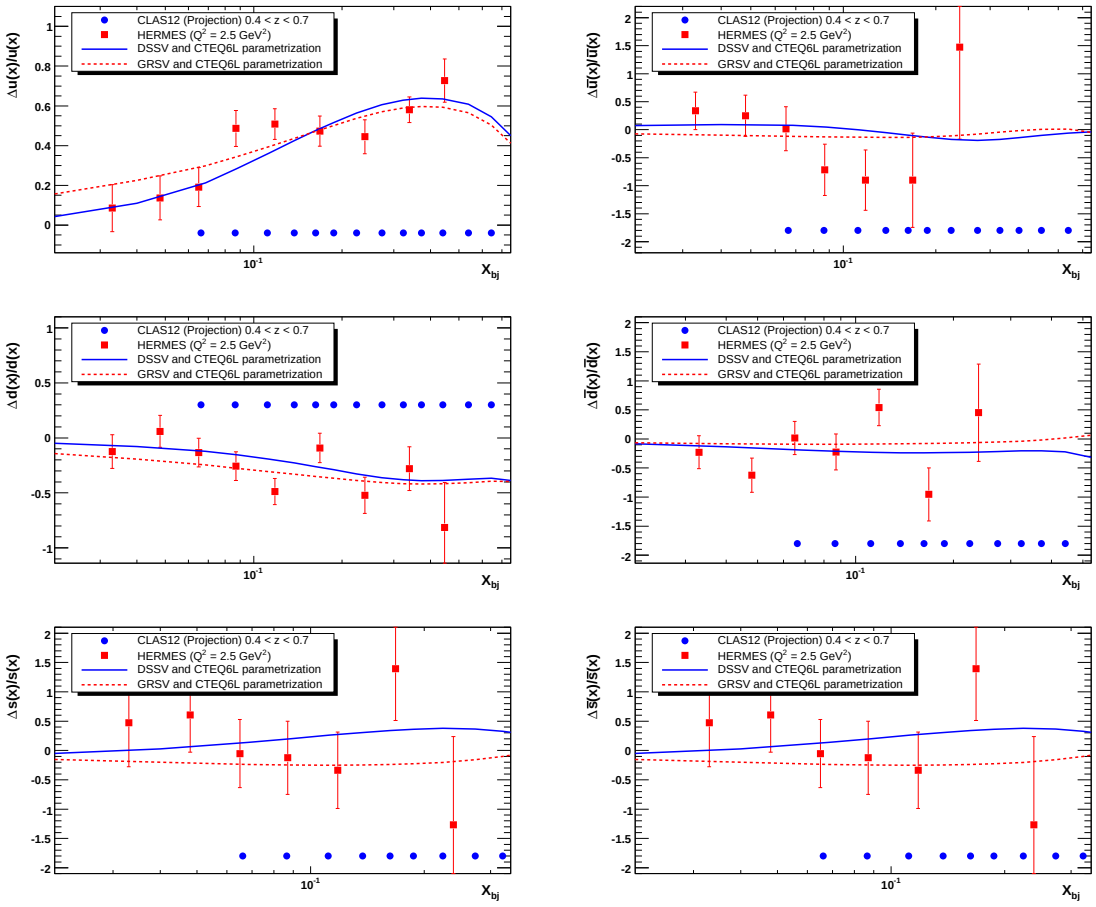

Fig. 22. Upper panel: Left (Right): Statistical projections for $\Delta u/u$ ($\Delta\bar{u}/\bar{u}$). Middle panel: Left (Right): Statistical projections for $\Delta d/d$ ($\Delta\bar{d}/\bar{d}$). Lower panel: Left (Right): Statistical projections for $\Delta s/s$ ($\Delta\bar{s}/\bar{s}$).

errors from the various contributions discussed in the previous Section in quadrature. They are listed in Table 3. Additional contributions to systematic error of measured asymmetries will come from uncertainties of unpolarized structure functions and also attenuation of hadrons in nuclear environment, which are a subject of a separate study (proposal E12-06-117 [34] on nuclei). The deuterium projections for double spin asymmetries are shown in Fig 18. The theory curves are obtained using CTEQ6L for the unpolarized PDFs, DSSV parameterization [13] for polarized PDFs and DSS for the fragmentation functions. Figure 19 shows the statistical projections for $x\Delta Q$ and $x\Delta S$ using the isoscalar method for kaons, K_s^0 and pions. For the strange polarized PDF, one needs to check the data and determine the highest x value one can reach since the strange PDF is expected to vanish for x value around or higher than 0.3. The great wealth of data will allow us to extract individual flavor contributions to the nucleon spin. We start by extracting individual asymmetries for different hadrons (π^+, π^-, π^0, K^+, K^- and K_s^0) from both proton and deuteron. The projected statistical

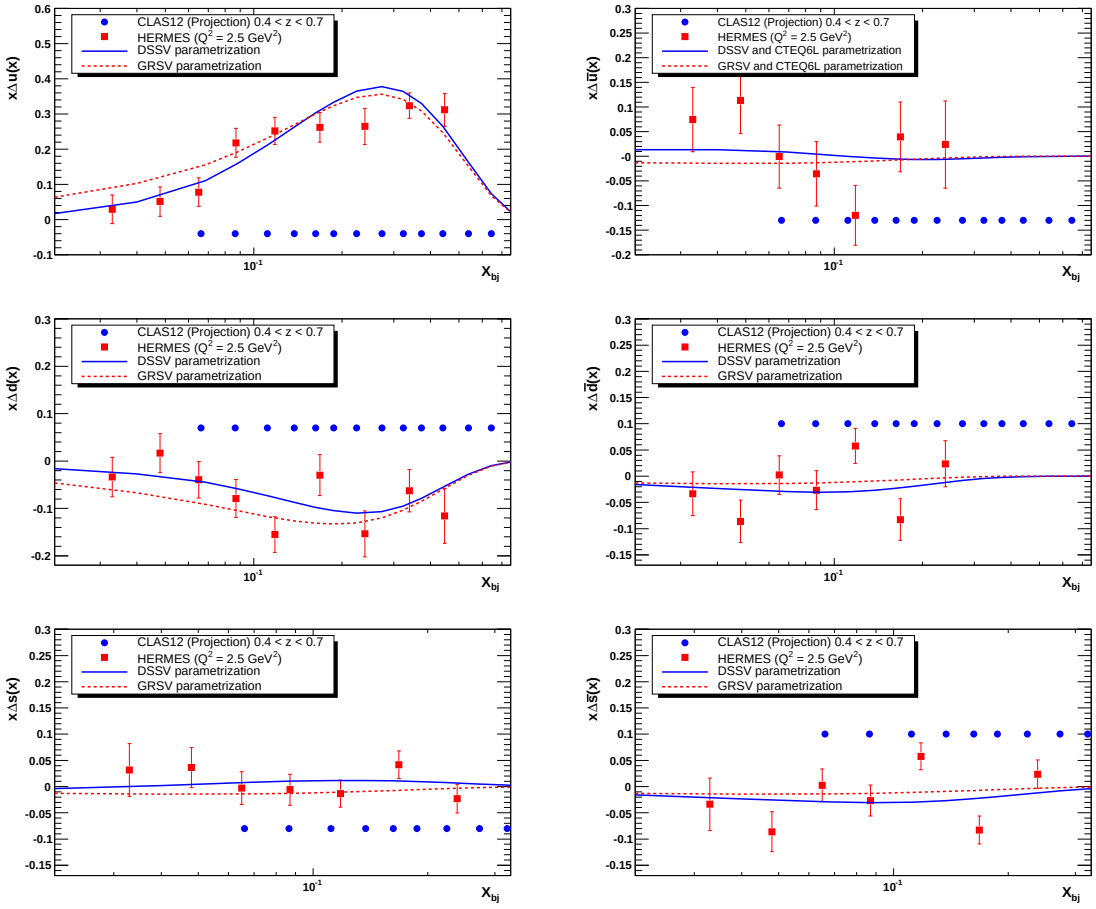

Fig. 23. Upper panel: Left (Right): Statistical projections for $x\Delta u$ ($x\Delta\bar{u}$). Middle panel: Left (Right): Statistical projections for $x\Delta d$ ($x\Delta\bar{d}$). Lower panel: Left (Right): Statistical projections for $x\Delta s$ ($x\Delta\bar{s}$).

precision is shown in Figs. 20 and 21. Using those asymmetries and purities from Monte Carlo, one can extract $\Delta q/q$ as shown in Fig. 22 as well as $x\Delta q$ (see Fig. 23). The statistical projections for $x(\Delta\bar{u} - \Delta\bar{d})$ are shown in Fig. 24. As one can seen we can measure it with unprecedented precision. Answering the question wether or not the light sea is not symmetrically polarized.

8 Beam Time Request and Summary

In this proposal, we are presenting a complete program for the study individual quark contribution to the nucleon spin. It represents a giant step in this field since we are benefiting from the successful combination of the high luminosity and the large acceptance offered by CLAS12. These measurements will also benefit from the knowledge

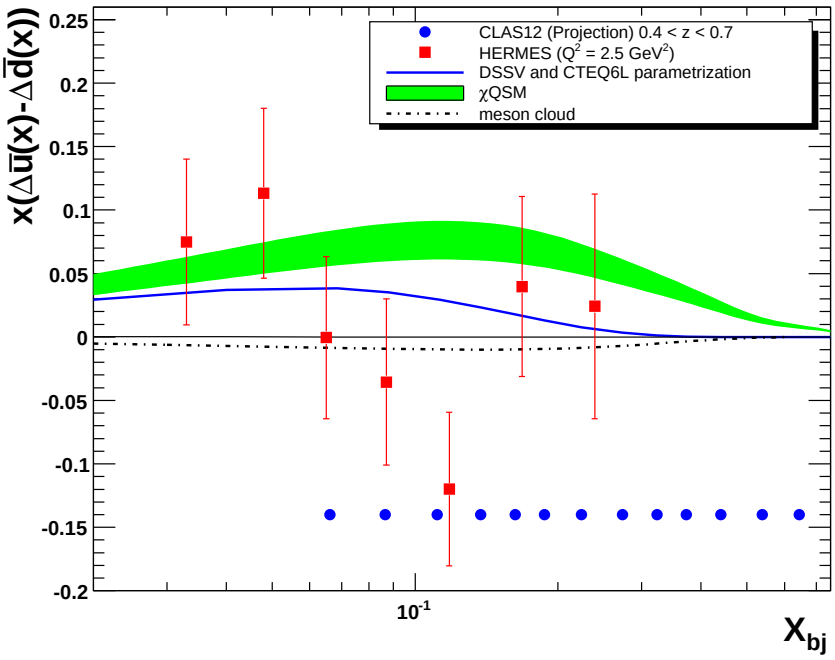

Fig. 24. Statistical projections for $x(\Delta\bar{u} - \Delta\bar{d})$.

and experience accumulated during more than a decade by HERMES collaboration. Measuring multiplicities in the same kinematical range as the semi inclusive asymmetries is the best way to reduce the systematics in the quark flavor decomposition. In addition to the fact that these multiplicities will constitute a valuable database for constraining the fragmentation functions parameterizations. Identifying several hadron species (π^+, π^-, π^0, K^+, K^- and K^0_s) in the final state is also an important element of success. In the x range between 0.05 and 0.7, we expect to measure with unprecedented precision the individual light flavor polarization using different methods that have different sensitivities and also systematics. We will be able to make no assumption in the six flavor decomposition extraction. For the first time, all six flavors (Δu, Δd, Δs, $\Delta\bar{u}$, $\Delta\bar{d}$, $\Delta\bar{s}$) can be extracted independently. We will also be able to precisely measure the most debatable quantity $\Delta\bar{u} - \Delta\bar{d}$ and answer the question whether or not the light sea is symmetrically polarized. These data will test several models that were able to describe the flavor asymmetry in the unpolarized quark sector. Using unpolarized deuteron data, we will also be able to measure the shape of the strange parton distribution functions and check the ansatz that they are average of the two light sea quark distributions.

One should also mention that we are aware of the fact that integrating over the momentum transverse P_T of the hadron could affect the helicity extraction of different quark flavors. Therefore much attention and careful studies will be devoted to that. They are the subject of two CLAS12 proposals which will be presented also in this PAC (PAC-34).

To achieve the goal of this proposal, we request a total of 54 days of an 11 GeV beam corresponding to 10^{35} cm^{-2} s^{-1} luminosity on a dual target with both unpolarized hydrogen and deuterium cells. These measurements can run simultaneously with the approved proposal E12-07-104 [21]. Two additional days were requested for diagnostic tests like empty target runs and straight-track runs and for interchanging the hydrogen and deuterium targets. In the last procedure, we would switch the liquids in each cell to test for any measurable effects due to the different target positions.

For the polarized measurements, we request a total of 80 days of 11 GeV, 10 nA highly polarized electron beam. 50 days of which are with longitudinally polarized deuterium and the remaining 30 days are for the longitudinally polarized hydrogen. These measurements can run concurrently with the approved proposals E12-06-109 [22] and E12-07-107 [23] and use the same commissioning time.

For this program to be successful, we need to enhance CLAS12 PID with a RICH detector. It will not only increase the kaon sample by a factor of 3 (in the right z range between 0.4 and 0.7) but it will also provide a major control over systematics as the kaon identification on the other "non-RICH" sectors will depend on the LTCC inefficiency. In addition to controlling the leak of pions and protons form different beam buckets, which is not possible with the time of flight. Moreover, a RICH detector will allow excellent particle identification since large and/or unknown particle misidentification will affect directly the systematics uncertainties in the quark flavor separation. Finally it will bring redundancy in CLAS12 PID that will benefit all.

References

[1] J. Pumplin et al. New generation of parton distributions with uncertainties from global QCD analysis. JHEP, 07:012, 2002.

[2] A. Kayis-Topaksu et al. Measurement of topological muonic branching ratios of charmed hadrons produced in neutrino induced charged- current interactions. Phys. Lett., B626:24–34, 2005.

[3] P. Astier et al. Neutrino production of opposite sign dimuons in the NOMAD experiment. Phys. Lett., B486:35–48, 2000.

[4] P. Vilain et al. Leading-order QCD analysis of neutrino induced dimuon events. Eur. Phys. J., C11:19–34, 1999.

[5] C. Peterson, D. Schlatter, I. Schmitt, and Peter M. Zerwas. Scaling Violations in Inclusive e+ e- Annihilation Spectra. Phys. Rev., D27:105, 1983.

[6] J. Ashman et al. Measurement of the Ratios of Deep Inelastic Muon - Nucleus Cross-Sections on Various Nuclei Compared to Deuterium. Phys. Lett., B202:603, 1988.

[7] A. Airapetian et al. Flavor decomposition of the sea quark helicity distributions in the nucleon from semi-inclusive deep- inelastic scattering. Phys. Rev. Lett., 92:012005, 2004.

[8] A. Airapetian et al. Measurement of Parton Distributions of Strange Quarks in the Nucleon from Charged-Kaon Production in Deep-Inelastic Scattering on the Deuteron. Phys. Lett., B666:446–450, 2008.

[9] M. Gluck, E. Reya, M. Stratmann, and W. Vogelsang. Models for the polarized parton distributions of the nucleon. Phys. Rev., D63:094005, 2001.

[10] J. Blumlein and H. Bottcher. QCD analysis of polarized deep inelastic scattering data and parton distributions. Nucl. Phys., B636:225–263, 2002.

[11] B. Dressler, K. Goeke, Maxim V. Polyakov, and C. Weiss. Flavor asymmetry of polarized antiquark distributions and semi-inclusive DIS. Eur. Phys. J., C14:147–157, 2000.

[12] Fu-Guang Cao and A. I. Signal. Non-perturbative structure of the polarized nucleon sea. Phys. Rev., D68:074002, 2003.

[13] Daniel de Florian, Rodolfo Sassot, Marco Stratmann, and Werner Vogelsang. Global Analysis of Helicity Parton Densities and Their Uncertainties. Phys. Rev. Lett., 101:072001, 2008.

[14] M. Alekseev et al. The Polarised Valence Quark Distribution from semi- inclusive DIS. Phys. Lett., B660:458–465, 2008.

[15] A Hillenbrand. Measurement and Simulation of the Fragmentation Process at HERMES. Ph.D. Thesis, Erlangen Univ, Germany , 2005.

[16] Stephen Scott Adler et al. Mid-rapidity neutral pion production in proton proton collisions at s**(1/2) = 200-GeV. Phys. Rev. Lett., 91:241803, 2003.

[17] John Adams et al. Forward neutral pion production in p+p and d+Au collisions at s(NN)**(1/2) = 200-GeV. Phys. Rev. Lett., 97:152302, 2006.

[18] I. Arsene et al. Production of Mesons and Baryons at High Rapidity and High Pt in Proton-Proton Collisions at sqrt(s) = 200 GeV. Phys. Rev. Lett., 98:252001, 2007.

[19] Yoshinori Fukao. The overview of the spin physics at RHIC-PHENIX experiment. AIP Conf. Proc., 842:321–323, 2006.

[20] Daniel de Florian, Rodolfo Sassot, and Marco Stratmann. Global analysis of fragmentation functions for pions and kaons and their uncertainties. Phys. Rev., D75:114010, 2007.

[21] G.P. Gilfoyle et al. Measurement of the Neutron Magnetic Form Factor at High Q^2 Using the Ratio Method on Deuterium . JLab Experiment E12-07-104, 2007.

[22] S. Kuhn et al. The Longitudinal Spin Structure of the Nucleon . JLab Experiment E12-06-109, 2006.

[23] H. Avakian et al. Studies of Spin-Orbit Correlations with Longitudinally Polarized Target. JLab Experiment E12-07-107, 2007.

[24] J. Lachniet et al. A Precise Measurement of the Neutron Magnetic Form Factor GMn in the Few-GeV2 Region. 2008.

[25] F. Garibaldi et al. A proximity focusing RICH detector for kaon physics at Jefferson Lab Hall A. Nucl. Instrum. Meth., A502:117–122, 2003.

[26] M. Iodice et al. Performance and results of the RICH detector for kaon physics in Hall A at Jefferson Lab. Nucl. Instrum. Meth., A553:231–236, 2005.

[27] F. Garibaldi et al. Hyper nuclei measurements. JLab Experiment E94-107, 1994.

[28] Application Software Group. GEANT - Detector Description and Simulation Tool. CERN Program Library Long Writeup W501, WWW://wwwinfo.cern.ch/asdoc/*geant_html*3/geantall.html, 2003.

[29] P. Rossi et al. RICH Detector for CLAS12. http://www.jlab.org/∼rossi/rich/*rich_v*2.pdf, 2008.

[30] K. V. Dharmawardane et al. Measurement of the x- and q^2-dependence of the asymmetry a_1 on the nucleon. Phys. Lett., B641:11–17, 2006.

[31] H. Avakian and P. Bosted. Mc-generator for dis studies with clas12. 2006.

[32] L. Mankiewicz, A. Schafer, and M. Veltri. Pepsi: A monte carlo generator for polarized leptoproduction. Comput. Phys. Commun., 71:305–318, 1992.

[33] Daniel de Florian, Rodolfo Sassot, and Marco Stratmann. Fragmentation functions for pions, kaons, protons and charged hadrons. J. Phys. Conf. Ser., 110:022045, 2008.

[34] K. Hafidi et al. Quark propagation and hadron formation. JLab Experiment E12-06-117, 2006.

9 Appendix A

x_{bj}	N^{DIS}	N^{π^+}	N^{π^-}	N^{π^0}	N^{K^+}	N^{K^-}	$N^{K_s^0}$
0.0746	222594	10856	6624	10120	1932	736	920
0.0900	106565486	5298924	3186696	4368068	1056436	391828	553196
0.1124	129891212	6917020	3805212	5448148	1362520	397532	608856
0.1372	116042222	6995128	3309332	5295888	1246232	317860	463036
0.1615	104782940	6380844	2709952	4725304	944564	235888	364320
0.1863	95019900	4905992	2127868	3690120	545376	116288	257416
0.2222	163779136	6261888	2988896	4905440	582268	42044	380420
0.2729	132519468	4211852	2210944	3347512	339756	4784	207276
0.3121	35802582	1114396	581256	848976	76360	0	28152

Table 4
The expected number of DIS, π^+, π^-, π^0, K^+, K^- and K_s^0 ($0.5 < z < 0.6$ and $1.3\ GeV^2 < Q^2 < 1.6\ GeV^2$) on unpolarized proton target

x_{bj}	N^{DIS}	N^{π^+}	N^{π^-}	N^{π^0}	N^{K^+}	N^{K^-}	$N^{K_s^0}$
0.2425	3315450	177652	85376	133860	38088	8188	15088
0.2771	22231846	1256904	567640	926900	258152	45632	98072
0.3240	22200750	1417720	547584	1008320	263212	42412	86112
0.3720	17732264	1128104	382904	779332	165600	26220	56764
0.4392	24254420	1035920	426604	768292	106812	10948	62376
0.5380	11849416	360088	178112	273056	34040	644	17756
0.6230	176732	5520	2208	4784	368	0	184

Table 5
The expected number of DIS, π^+, π^-, π^0, K^+, K^- and K_s^0 ($0.5 < z < 0.6$ and $4.0\ GeV^2 < Q^2 < 5.0\ GeV^2$) on unpolarized proton target

x_{bj}	N^{DIS}	N^{π^+}	N^{π^-}	N^{π^0}	N^{K^+}	N^{K^-}	$N^{K_s^0}$
0.0746	254544	10272	9216	10080	3072	960	1152
0.0901	119033856	5744256	3792768	4840608	1114080	458592	601152
0.1122	143092608	7377696	4565856	5952192	1401504	484704	674016
0.1370	125799600	7104288	4122048	5599200	1178976	372288	522816
0.1615	111521280	6022560	3581280	4888896	851136	270144	393024
0.1864	99219168	4338624	2765280	3706752	497760	136128	259776
0.2225	166834368	5415648	3366720	4735680	590112	39552	325728
0.2733	130399344	3478176	2411136	3124608	360096	4800	169152
0.3118	34387296	895872	642816	775008	86112	0	27552

Table 6
The expected number of DIS, π^+, π^-, π^0, K^+, K^- and K_s^0 ($0.5 < z < 0.6$ and $1.3\ GeV^2 < Q^2 < 1.6\ GeV^2$) on unpolarized deuteron target

x_{bj}	N^{DIS}	N^{π^+}	N^{π^-}	N^{π^0}	N^{K^+}	N^{K^-}	$N^{K_s^0}$
0.2422	3399120	170976	102144	134592	40512	7776	15744
0.2769	22351440	1220640	649824	939168	252672	47040	99360
0.3239	21586224	1302624	633888	962880	234528	37056	84672
0.3717	16875312	957792	455232	725280	142272	23616	56736
0.4401	22565280	840768	463680	685440	99072	9216	54816
0.5374	10552080	276672	181824	228096	29376	576	13056
0.6230	156960	4608	3264	3552	384	0	0

Table 7
The expected number of DIS, π^+, π^-, π^0, K^+, K^- and K_s^0 ($0.5 < z < 0.6$ and $4.0\ GeV^2 < Q^2 < 5.0\ GeV^2$) on unpolarized deuteron target

x_{bj}	N^{DIS}	N^{π^+}	N^{π^-}	N^{π^0}	N^{K^+}	N^{K^-}	$N^{K^0_s}$
0.0746	11643	635	239	557	107	39	68
0.0901	5587641	286099	158035	229052	57824	19701	28474
0.1124	6795006.9	373302	186201	285077	73530	20308	30391
0.1372	6036890	372774	159775	276377	67144	16254	22885
0.1615	5408261	336652	132127	244734	50005	12391	18650
0.1863	4865095	255375	104650	190059	28195	6215	13139
0.2222	8326608	324285	149174	250764	30166	2200	19545
0.2727	6680424	216499	110983	169492	17589	244	10288
0.3119	1803969	56802	28577	42816	3804	0	1334

Table 8
The expected number of DIS, π^+, π^-, π^0, K^+, K^- and K^0_s ($0.5 < z < 0.6$ and $1.3\ GeV^2 < Q^2 < 1.6\ GeV^2$) on polarized proton target (positive helicity)

x_{bj}	N^{DIS}	N^{π^+}	N^{π^-}	N^{π^0}	N^{K^+}	N^{K^-}	$N^{K_s^0}$
0.2425	211208	11613	4630	8415	2484	537	870
0.2770	1432373	84905	31829	59433	17471	2860	6039
0.3236	1419244	95286	29496	64758	17716	2757	5315
0.3718	1118753	74049	21721	49931	10777	1608	3687
0.4383	1498897	65755	25207	47657	6713	733	3775
0.5378	711211	21902	10464	16220	2063	48	1041
0.6230	10582	356	112	308	39	0	9

Table 9
The expected number of DIS, π^+, π^-, π^0, K^+, K^- and K_s^0 ($0.5 < z < 0.6$ and $4.0\ GeV^2 < Q^2 < 5.0\ GeV^2$) on polarized proton target (positive helicity)

x_{bj}	N^{DIS}	N^{π^+}	N^{π^-}	N^{π^0}	N^{K^+}	N^{K^-}	$N^{K^0_s}$
0.0746	12770	540	500	515	135	45	75
0.0901	6000205	293075	189120	244325	57300	21980	30605
0.1122	7260260	375270	226970	302820	72960	22890	34310
0.1371	6405300	363230	207770	285845	61745	18070	26580
0.1614	5695100	311530	180460	252320	45815	13410	20310
0.1864	5082730	226250	140950	192355	26175	6785	13525
0.2223	8563310	285365	175880	246895	30975	2005	17355
0.2731	6716780	182230	126125	163635	18960	195	9135
0.3121	1778800	47385	33090	40410	4330	0	1455

Table 10
The expected number of DIS, π^+, π^-, π^0, K^+, K^- and K^0_s ($0.5 < z < 0.6$ and $1.3\ GeV^2 < Q^2 < 1.6\ GeV^2$) on polarized deuteron target (positive helicity)

x_{bj}	N^{DIS}	N^{π^+}	N^{π^-}	N^{π^0}	N^{K^+}	N^{K^-}	$N^{K_s^0}$
0.2421	197135	9695	5625	7900	2435	505	935
0.2769	1314730	70730	38500	55305	15060	2900	6090
0.3240	1281305	76185	37665	57610	14205	2200	5340
0.3713	1005320	57550	27615	43600	8825	1495	3665
0.4407	1343315	52020	28200	42295	6070	480	3505
0.5365	630545	17125	11070	13890	1835	35	815
0.6230	9565	240	200	205	25	0	0

Table 11
The expected number of DIS, π^+, π^-, π^0, K^+, K^- and K_s^0 ($0.5 < z < 0.6$ and $4.0\ GeV^2 < Q^2 < 5.0\ GeV^2$) on polarized deuteron target (positive helicity)

x_{bj}	N^{DIS}	N^{π^+}	N^{π^-}	N^{π^0}	N^{K^+}	N^{K^-}	$N^{K^0_s}$
0.0746	12019	518	464	518	102	39	34
0.0900	5740732	277204	180724	235297	54479	21951	30332
0.1124	7012993	362006	218309	294084	71310	21951	34337
0.1372	6298901	370842	192020	286602	65340	17540	26337
0.1615	5730620	341659	155956	257590	50406	12684	20078
0.1863	5235933	266152	121555	202216	29784	6146	14229
0.2223	9083825	341385	168558	270705	31736	2273	20899
0.2731	7406970	231238	124054	186367	18528	264	11745
0.3124	2002000	61662	33217	47437	4317	0	1662

Table 12
The expected number of DIS, π^+, π^-, π^0, K^+, K^- and K^0_s ($0.5 < z < 0.6$ and $1.3\ GeV^2 < Q^2 < 1.6\ GeV^2$) on polarized proton target (negative helicity)

x_{bj}	N^{DIS}	N^{π^+}	N^{π^-}	N^{π^0}	N^{K^+}	N^{K^-}	$N^{K_s^0}$
0.2425	141237	7271	4445	5819	1569	337	738
0.2773	930968	48709	28518	39105	9970	1995	4386
0.3244	940792	55428	28714	42435	10264	1750	3843
0.3722	766263	45877	18987	32919	6831	1178	2352
0.4401	1079452	44366	20146	34019	4645	430	2855
0.5382	548433	16376	8469	12806	1559	24	850
0.6230	8205	229	127	205	0	0	14

Table 13
The expected number of DIS, π^+, π^-, π^0, K^+, K^- and K_s^0 ($0.5 < z < 0.6$ and $4.0\ GeV^2 < Q^2 < 5.0\ GeV^2$) on polarized proton target (negative helicity)

x_{bj}	N^{DIS}	N^{π^+}	N^{π^-}	N^{π^0}	N^{K^+}	N^{K^-}	$N^{K^0_s}$
0.0746	13745	535	460	540	185	60	45
0.0900	6399155	305285	205965	259905	58750	25795	32015
0.1122	7645220	393240	248640	317205	73035	27600	35900
0.1370	6698825	376805	221615	297410	61070	20710	27885
0.1615	5921700	315825	192595	256940	42845	14730	20635
0.1865	5252600	225695	147105	193770	25675	7395	13535
0.2228	8815270	278770	174825	246410	30495	2120	16575
0.2734	6866485	180080	125040	161850	18550	305	8490
0.3114	1803210	45940	33870	40325	4640	0	1415

Table 14
The expected number of DIS, π^+, π^-, π^0, K^+, K^- and K^0_s ($0.5 < z < 0.6$ and $1.3\ GeV^2 < Q^2 < 1.6\ GeV^2$) on polarized deuteron target (negative helicity)

x_{bj}	N^{DIS}	N^{π^+}	N^{π^-}	N^{π^0}	N^{K^+}	N^{K^-}	$N^{K_s^0}$
0.2423	156940	8115	5015	6125	1785	305	705
0.2769	1013545	56425	29195	42525	11265	2000	4260
0.3238	967260	59505	28365	42695	10230	1665	3480
0.3722	752525	42220	19810	31950	6000	970	2250
0.4396	1007235	35565	20100	29110	4255	480	2205
0.5384	468630	11695	7875	9875	1225	25	545
0.6230	6785	240	140	170	20	0	0

Table 15
The expected number of DIS, π^+, π^-, π^0, K^+, K^- and K_s^0 ($0.5 < z < 0.6$ and $4.0\ GeV^2 < Q^2 < 5.0\ GeV^2$) on polarized deuteron target (negative helicity)

x_{bj}	N^{DIS}	N^{π^+}	N^{π^-}	N^{π^0}	N^{K^+}	N^{K^-}	$N^{K_s^0}$
0.0662	6366232	986616	593362	818136	188734	77775	95658
0.0864	19422562	3140607	1740859	2533156	598061	207917	274930
0.1114	23502244	4067550	2022411	3159966	727568	216152	298485
0.1374	24328826	4289224	1965726	3269224	691338	181619	276945
0.1624	23865712	4009183	1765182	3030049	583054	132323	242470
0.1873	22786480	3557240	1540315	2697152	479342	90249	210475
0.2243	41142944	5855383	2562535	4453034	719754	105535	323414
0.2732	27840320	3798204	1638502	2864464	440295	52934	191639
0.3230	16302859	2204084	926102	1647646	250456	27066	107628
0.3730	9539397	1272842	526149	941188	142240	14039	61286
0.4409	8551333	1104523	451904	813250	120069	10557	51677
0.5391	2483161	299590	122044	218695	30983	2117	13310
0.6450	616570	66220	27838	48450	6748	190	2836

Table 16
The expected number of DIS, π^+, π^-, π^0, K^+, K^- and K_s^0 on polarized proton target (positive helicity)

x_{bj}	N^{DIS}	N^{π^+}	N^{π^-}	N^{π^0}	N^{K^+}	N^{K^-}	$N^{K_s^0}$
0.0662	6937071	1032914	693406	893803	193893	88689	111374
0.0864	20728264	3200079	2032308	2696404	596472	232098	310647
0.1114	24746318	4090460	2360099	3325082	715255	236172	334930
0.1374	25372532	4269884	2280969	3397302	669113	190773	300734
0.1624	24730274	3927706	2010934	3108895	554413	132748	254539
0.1873	23547130	3440765	1739656	2731749	447156	86895	219233
0.2243	42382764	5583499	2833344	4455846	653152	95002	327737
0.2732	27648396	3454990	1747475	2750258	371918	42645	180783
0.3230	15215386	1858850	934586	1472198	199223	19354	94469
0.3730	8333117	1002176	497132	788072	104998	9061	50332
0.4409	6751828	779490	387287	610487	79540	5872	37741
0.5391	1666634	179722	88831	139374	18264	968	8259
0.6450	325615	32572	15427	25740	3471	88	1359

Table 17
The expected number of DIS, π^+, π^-, π^0, K^+, K^- and K_s^0 on polarized proton target (negative helicity)

x_{bj}	$\delta A_1^{DIS}(x)$	$\delta A_1^{\pi^+}(x)$	$\delta A_1^{\pi^-}(x)$	$\delta A_1^{\pi^0}(x)$	$\delta A_1^{K^+}(x)$	$\delta A_1^{K^-}(x)$	$\delta A_1^{K_s^0}(x)$
0.0662	0.000053	0.000225	0.000371	0.000282	0.000523	0.001037	0.001690
0.0864	0.000035	0.000129	0.000211	0.000186	0.000298	0.000620	0.000952
0.1114	0.000036	0.000121	0.000202	0.000190	0.000288	0.000628	0.000929
0.1374	0.000041	0.000128	0.000216	0.000207	0.000316	0.000722	0.001030
0.1624	0.000045	0.000141	0.000240	0.000231	0.000364	0.000890	0.001174
0.1873	0.000051	0.000160	0.000272	0.000261	0.000424	0.001118	0.001338
0.2243	0.000043	0.000136	0.000229	0.000224	0.000375	0.001098	0.001163
0.2732	0.000053	0.000168	0.000283	0.000281	0.000478	0.001588	0.001471
0.3230	0.000065	0.000204	0.000347	0.000341	0.000591	0.002098	0.001784
0.3730	0.000079	0.000247	0.000422	0.000412	0.000723	0.002620	0.002224
0.4409	0.000075	0.000236	0.000407	0.000391	0.000704	0.002755	0.002054
0.5391	0.000119	0.000384	0.000661	0.000622	0.001177	0.005440	0.003374
0.6450	0.000198	0.000680	0.001143	0.001116	0.002101	0.011859	0.005677

Table 18
The projected errors on inclusive, π^+, π^-, π^0, K^+, K^- and K_s^0 spin asymmetries on proton target

x_{bj}	N^{DIS}	N^{π^+}	N^{π^-}	N^{π^0}	N^{K^+}	N^{K^-}	$N^{K^0_s}$
0.0685	6989185	1031940	706745	896735	197365	86785	108170
0.0881	21116056	3216525	2113555	2730470	596100	235835	307595
0.1126	25267664	4027390	2539255	3352155	699885	243075	338380
0.1374	25847896	4103500	2545765	3423215	645970	203145	306225
0.1623	25014150	3708535	2275625	3107495	546465	144070	259060
0.1873	23575404	3213795	1940150	2718625	448975	96365	215330
0.2241	41771604	5144780	3137260	4379315	675960	106955	316340
0.2730	27382396	3220955	1955590	2735235	399090	49210	182735
0.3229	15490410	1809475	1074015	1521480	218880	24120	100025
0.3728	8844055	1019140	599780	849910	124625	11665	54640
0.4406	7733875	867870	508420	721775	102570	8735	45080
0.5389	2175375	230815	133910	187125	25885	1630	11640
0.6447	524685	50470	29240	40500	5560	175	2430

Table 19
The expected number of DIS, π^+, π^-, π^0, K^+, K^- and K^0_s on polarized deuteron target (positive helicity)

x_{bj}	N^{DIS}	N^{π^+}	N^{π^-}	N^{π^0}	N^{K^+}	N^{K^-}	$N^{K^0_s}$
0.0685	7694955	1112375	805165	985525	205575	106935	121945
0.0881	22795176	3406005	2350635	2931430	617115	279150	331185
0.1126	26793524	4222745	2781120	3530195	707860	282665	354160
0.1374	26952630	4203735	2735650	3528105	637585	229170	312060
0.1623	25745556	3733300	2383805	3151030	524065	157935	257975
0.1873	23958504	3163755	1974350	2695565	426900	99685	207200
0.2241	41803860	4935110	3087440	4258055	630910	102920	289790
0.2730	26397476	2968950	1835150	2539945	355140	42550	157385
0.3229	14194050	1571505	950455	1327940	186165	18245	80940
0.3728	7650835	830415	493370	699010	95385	7835	41415
0.4406	6144455	644605	383890	537445	72945	4825	30700
0.5389	1480415	144520	86795	118685	15815	610	6490
0.6447	284280	25330	15335	20645	2930	60	965

Table 20
The expected number of DIS, π^+, π^-, π^0, K^+, K^- and K^0_s on polarized deuteron target (negative helicity)

x_{bj}	$\delta A_1^{DIS}(x)$	$\delta A_1^{\pi^+}(x)$	$\delta A_1^{\pi^-}(x)$	$\delta A_1^{\pi^0}(x)$	$\delta A_1^{K^+}(x)$	$\delta A_1^{K^-}(x)$	$\delta A_1^{K_s^0}(x)$
0.0685	0.000055	0.000239	0.000368	0.000290	0.000561	0.001027	0.001755
0.0881	0.000036	0.000137	0.000206	0.000192	0.000321	0.000621	0.000986
0.1126	0.000037	0.000130	0.000194	0.000197	0.000314	0.000622	0.000954
0.1374	0.000042	0.000139	0.000203	0.000214	0.000348	0.000717	0.001050
0.1623	0.000047	0.000156	0.000226	0.000242	0.000402	0.000895	0.001203
0.1873	0.000054	0.000179	0.000259	0.000277	0.000471	0.001151	0.001421
0.2241	0.000046	0.000155	0.000222	0.000242	0.000418	0.001171	0.001254
0.2730	0.000057	0.000196	0.000279	0.000308	0.000542	0.001758	0.001614
0.3229	0.000071	0.000242	0.000348	0.000381	0.000684	0.002368	0.002032
0.3728	0.000088	0.000298	0.000429	0.000468	0.000835	0.003160	0.002519
0.4406	0.000085	0.000289	0.000417	0.000449	0.000833	0.003318	0.002455
0.5389	0.000139	0.000480	0.000691	0.000741	0.001408	0.006803	0.003836
0.6447	0.000238	0.000860	0.001236	0.001315	0.002581	0.020512	0.007462

Table 21
The projected error on inclusive, π^+, π^-, π^0, K^+, K^- and K_s^0 spin asymmetries on deuteron target